ASSESSMENT OF ANTICORROSION AND ANTIFOULING PERFORMANCE OF EPOXY-CHITOSAN COATING USING COMPUTATIONAL SIMULATION TECHNIQUE

BY

IKECHUKWU, UZOCHUKWU NELSON

ACE-FUELS/20/MSc/11000106

A THESIS SUBMITTED TO THE

POSTGRADUATE SCHOOL, FEDERAL UNIVERSITY OF TECHNOLOGY, OWERRI

IN PARTIAL FULFILMENT OF THE REQUIREMENT FOR THE AWARD OF MASTER OF SCIENCE (M.Sc.) DEGREE IN CORROSION TECHNOLOGY

July, 2023

CERTIFICATION

This is to certify that this research was carried out and written by me, Ikechukwu, Uzochukwu Nelson, (Reg No: ACE-FUELS/20/MSc/11000106) a master's Degree student of the Department of Corrosion Technology at the Africa Centre of Excellence in Future Energies and Electrochemical Systems (ACE-FUELS), Federal University of Technology, Owerri (FUTO).

…… Date…31/08/23…

Engr. Dr. Innocent O. Arukalam
(Supervisor)

…… Date…14/09/23…

Engr. Dr. Chigoziri N. Njoku
(Co-supervisor)

…… Date…10/8/2023…

Dr. C.O. Akalezi
(Program Coordinator)

…… Date…14/9/23…

Prof. Emeka E. Oguzie
(Centre Leader)

…… ….. Date……

Prof. B.O. Esonu
(Dean, Postgraduate School)

…… Date…10 August, 2023…

Prof. P. C. Okafor
(External Examiner)

DEDICATION

This work is dedicated to Almighty God, the giver of knowledge and whose grace sustained me throughout this study.

ACKNOWLEDGMENT

With a sense of gratitude, I wish to acknowledge the invaluable contributions, supports, encouragements and guidance of my supervisors, Engr. Dr. Innocent O. Arukalam and Dr. Chigoziri N. Njoku which helped me throughout the period of my research and thesis writing.

My gratitude also goes to my class adviser, Engr. Dr. Simeon Nwanonenyi, research coordinator, Dr. (Mrs) Kanayo Oguzie and all ACE-FUELS lecturers for the knowledge they imparted to me during my studies. In a special way, I wish to appreciate the Centre Leader, Prof. Emeka E. Oguzie for his fatherly role. Furthermore, the funding from the World Bank is greatly acknowledged.

The supports from my parents, Mr. & Mrs. Edmund Okonkwo, and uncle, Rev. & Mrs Charles Nwoke in the course of my studies are well appreciated. My siblings and friends are also acknowledged for their supports.

TABLE OF CONTENTS

LIST OF TABLES

LIST OF FIGURES

ABSTRACT

Assessment of anticorrosion and antifouling performance of epoxy-chitosan coating in simulated marine water has been conducted using quantum chemical computations and molecular dynamic simulation technique. The objective was to gain insights into the molecular/atomistic level of the coating/metal interface to be able to design high performance anticorrosion and antifouling epoxy nanocomposite coatings for marine application. The coating formulation was based on diglydicyl ether of bisphenol A (DGEBA) epoxy cured with 1,3 benzenediamine (BDA). Chitosan biopolymer nanoclusters were used as filler. Two different silane additives; tetraethoxysilane (TEOS) and (3-Aminopropyl) trimethoxy silane (APTES) were used as hydrophobic modifiers. Mild steel and 3.5 wt.% NaCl solution were used as substrate and corrodent, respectively. L-DOPA which is a major component of adhesive protein secreted by mussel was used as a foulant. Chitosan nanocluster was modified with each of the two different silane modifiers (TEOS, APTES), and then incorporated into the epoxy coating formulation. Computational results showed that the obtained quantum chemical parameters (EHOMO, ELUMO, energy gap, global softness, electronegativity, etc) are related to high corrosion protective capability. The adsorption energies (E_{ads}) of the silane-modified chitosan/epoxy coatings were observed to be higher than the unsalinized chitosan/epoxy and plain epoxy coatings. It was also observed that the adsorption energy increased with the addition of silane modified chitosan nanocluster in the order: APTES>TEOS>chitosan. MD simulation was again used to probe antifouling potential of DGEBA-BDA/ chitosan and silane modified chitosan nanocluster by studying the interaction between the composite coating and L-DOPA which is a major component of adhesive protein secreted by mussel. Results showed that the adsorption energy reduced in the presence of silane modified chitosan nanocluster in the order: APTES<TEOS<chitosan. This implies that DGEBA-BDA (epoxy coating) filled with silane modified chitosan nanoparticle has the potential to perform as a good anticorrosion and antifouling coating for mild steel in marine environment with APTES modified chitosan performing better both in anticorrosion and antifouling performance. Thus, it is believed that the results of this study will be useful in the design of epoxy/chitosan coating for mild steel in marine environment.

Keywords: Anticorrosion, Antifouling, Computational simulation technique, Epoxy coating, Silane-modified chitosan.

CHAPTER ONE

INTRODUCTION

1.1 Background of Study

Metallic materials are the most widely used materials in the field of engineering. It finds its applications in areas such as in mechanical systems, transportation vehicles, electronic equipment, construction industries (Rathi, 2017), oil and gas pipelines and facilities (Umoren et al., 2020) and also in the construction of marine assets or vessels (Urbahs et al., 2018), nuclear power and fossil fuel power plants, chemical processing, mining and metal-processing equipment (Suleiman & El, 2015), etc. The reason for the wide applications of metals is due to their good mechanical strength and durability. However, their susceptibility to corrosion damage has restricted their application.

Notably, corrosion phenomenon which is defined as the degradation or deterioration of metals and their alloys from thermodynamically unstable refined state to chemically stable state such as oxides, sulphides have wrecked a lot of havoc in industries. In practice, it occurs when metals interact with their operating environments, leading to changes in both physical and mechanical properties, and thus reduces efficiency of metallic components (Hari Kumar & Karthikeyan, 2020). It also proceeds through an electrochemical process where electrons are lost due to oxidation at the anode and gained at the cathode via reduction process. More often than not, it is spontaneous due to the inherent tendency of metallic materials to return to their natural states. The oxidation of these metallic materials occurs when exposed to corrosive environment, and this makes them lose their malleable and ductile characteristics. This is a precursor to existential mechanical failures, with examples seen in the collapse of some important engineering constructions like bridges, oil pipelines, refinery facilities, buildings resting on metallic stands, etc. (Obi-Egbedi & Ojo, 2015).

Furthermore, it is important to state that the challenges caused by corrosion damage have become a global problem with their attendant effect on the global economy and human safety. Thus, presently, the annual global cost of corrosion is estimated at US$2.5 trillion which is equivalent to 3.4% of the world's gross domestic product (GDP) (Umoren et al., 2020). The losses incurred from this corrosion menace are grouped into direct and indirect losses. The direct losses cover the cost of replacing corroded or failed metallic structures and machinery, painting and repainting of metallic structures, using highly corrosion-resistant materials and alloys, etc. Situations such as plant shutdowns as well as the loss of products and reduction in materials' efficiency belong to the indirect cost (Umoren et al., 2020).

Corrosion has also posed a lot of threats to human lives. For example, the explosion of Qingdao oil pipeline that took place on 22 November 2013, in Qingdao, China is a remarkable one. In that incident, more than 62 people were killed and 136 were reportedly injured. The cause of that incident was traced to ignition of vapours produced from oil leaking from a corroded underground pipeline (Umoren et al., 2020).

It is important to point out that corrosion does not just happen. Some environments facilitate the corrosion of metals, and they include acidic environment which is typical to the oil and gas industries (Afia et al., 2011). Processes such as acid cleaning, acid descaling, oil well acidification and other petrochemical processes involve the use acids (Afia et al., 2011) which can eventually lead to the corrosion of the metals deployed to such environment.

On the other hand, some metallic components and equipment such as marine vessels, subsea oil rig facilities, offshore oil and gas platforms, etc. are deployed to marine environment which has been described as harsh and highly corrosive environment for metals and alloys because of the presence of micro-

organisms plus high chloride and sulphate contents (Urbahs et al., 2018). The attachment and settlement of micro and/or macro organisms on ship hulls, a phenomenon known as biofouling (Xie et al., 2021) has been a major problem to the shipping industries. The effect is enormous and ranges from increasing ship's drag through reduction of speed to increased fuel consumption and consequently increase in the emission of harmful gasses to the atmosphere. Also, the metabolic activities of these microorganisms attached to the surface of ship hulls tend to set up an electrochemical system as well as a change in the pH of the medium leading to corrosion, a phenomenon known as microbial influenced corrosion (Chaparro et al., 2020).

It should also be noted that marine fouling facilitates corrosion, and corrosion in the marine environment has posed a big challenge to the shipping industries. This is due to the cost associated with the replacement of the corroded parts of ships and its life-threatening consequences. It has been estimated that the loses due to the corrosion of marine transport vessels from the time of construction to operation is about 50-80 billion USD (Urbahs et al., 2018) and this constitutes about 3% of the world's GDP. Thus, there is need to mitigate the corrosion of metals served in the marine environment.

Much effort has been made to mitigate or control marine fouling as well as microbial influenced corrosion. Primarily, this involves hindering or controlling the growth and activities of microorganisms on the surface of metals (Chaparro et al., 2020). Among the several techniques of controlling biofouling and microbial influenced corrosion, the use of protective coatings have been adjudged as one of the best strategies (Arukalam, et al., 2021). However, in recent past, biocides such as tributyltin compounds and organometallic copper (Lejars et al., 2011; Razavi et al., 2019) were incorporated into protective coatings to prevent or discourage the settlement of microorganisms on metal substrates (Lejars et al., 2011; Xie et al., 2020), but they have been banned due to their toxicity to aquatic

lives. Hence, there is need to develop an eco-friendly anticorrosion and anti-fouling or foul release coatings suitable for the protection of marine vessels.

In view of this, so many researchers have developed and still developing methods to control or mitigate corrosion. In acidic environment, the use of corrosion inhibitors and protective coatings have thrived(Afia et al., 2011; Arukalam, et al., 2021). Nonetheless, in order to effectively probe the anticorrosion and antifouling performance of coatings on metal surfaces, the knowledge of interface property is necessary. Nonetheless, investigation of interface property of coatings on metal surfaces has for long remained a herculean task. This is because interfacial bonding is a molecular/atomic-level interaction activity. Though many experimental methods have been proposed to probe transitions in metal surface–polymeric coating interface, there are still some serious weak points associated with experimental investigations. The observed weak points manifest in deterioration of the surfaces under probe. But to better understand the interface properties of the coating and metal from a molecular/atomic perspective, non-destructive evaluation is desired.

Consequently, computational modelling and simulation techniques, which have proven to be powerful tools for investigating interfacial interactions at a molecular/atomic level, and provide a detailed picture of interfacial evolutions are recommended(Dagdag, et al., 2020; Uwakwe et al., 2016). Molecular dynamics (MD) and Monte Carlo (MC) simulation can give detailed information on the atomic level about interactional developments and time evolution of a given complex system (Dagdag, et al., 2020). The quantum chemical studies are considered a powerful tool to determine the most stable, conformable structure of the coating molecules and their electronic properties. Anticorrosion and antifouling coating mechanisms can be determined by analysing the active sites of coating using DFT (Density Functional Theory) methods.

1.2 Research problem

Coating/metal interface properties play a great role in determining the service properties of coated metal structures deployed for operation in corrosion and fouling prone environment. But interfacial property is a molecular/atomistic level phenomenon, and the use of experimental techniques alone has not been sufficient to properly assess it because of observed material's tendency to deterioration during in-situ investigation. To better understand the interface properties of coating/metal system from a molecular/atomistic perspective, computational simulation technique has proven to be a powerful tool and provides detailed pictures of interfacial evolution. Thus, there is need to deploy this technique for determination of interface properties of silane-modified epoxy-chitosan coating/metal system to properly understand their mechanistic actions for anticorrosion and antifouling processes.

In addition, the corrosion and fouling menaces often observed on coated structures are due to hydrophilic nature of the coatings which allow seepage of corrodents and provides anchorage for attachment of foulants. Therefore, to enhance reliability and stability of coated metal structures, the use of hydrophobic materials/surfaces is considered to be one of the best approaches due to their numerous advantages which include self-cleaning, drag reduction, anti-fouling and corrosion resistance properties. To engineer a sustainable superhydrophobic material/surface, knowledge of nanoscopic intermolecular interactions within liquid-solid interface is needed. Thus, molecular dynamics (MD) simulations provide the numerical solution of the classic equations of physical motion (Newton's equations) of atoms and molecules and are used for predicting the surface tensions of liquids and solid surfaces and contact angles of liquid nanodroplets since these terms cannot be easily measured experimentally.

1.3 Aim and Objectives of study

The aim of this study is to assess the anticorrosion and antifouling performance of epoxy-chitosan coating using computational simulation technique.

The objectives are to:

1. assess the anticorrosion and antifouling performances of silane-modified epoxy-chitosan coating by analysing its active sites and adsorption mechanism using computational simulation technique.
2. determine the effect of chitosan nanoparticles on the anticorrosion and antifouling performance of the epoxy-chitosan coating by use of computational simulation technique.
3. determine the effect of different silane additives on the anticorrosion and antifouling performances of the epoxy-chitosan coating by use of computational simulation technique.
4. design robust silane-modified epoxy-chitosan coatings for corrosion and fouling protection of mild steel deployed in 3.5wt% NaCl and 3.5wt% NaCl/foulant operating media by use of computational simulation technique.

1.4 Justification

High barrier nanostructured coatings have been reported to be one of the eco-friendliest, sustainable and facile way of protecting metallic structures deployed for marine services (Dennis et al., 2015). In addition, preliminary investigation (Arukalam et al., 2021) reveals that some of our biomass provide fillers and resinous liquids which are precursors to synthesis of biomaterials used for surface properties improvement. Silane additives have also been proven to exhibit low surface energy which helps to impart high barrier performance (Arukalam et al., 2021). Hence, it is believed that the use of silane surface chemistry modifiers and chitosan biopolymer nanoparticles obtained from local

biomass resources would effectively and efficiently serve to enhance epoxy coating's surface properties and ensure durability.

1.5 Scope of study

The study is restricted to the use of density functional theory (DFT) and Molecular Dynamics (MD) simulation techniques contained in Materials Studio software. This involves sketching and simulation of the following molecules and structures:

(i) Mild steel framework which was used as a metal substrate.

(ii) An epoxy resin (diglycidyl ether Bisphenol A, DGEBA) as a coating resin, and 1,3 benzenediamine as a curing agent.

(iii) Chitosan nanocluster, as a surface roughening additive.

(iv) Silane additives – Tetraethoxy silane, (3- Aminopropyl) triethoxy silane. These serve to modify the surface chemistry of the coating.

(v) Water nanodroplets on silane-modified epoxy-chitosan coated surface.

(vi) Seawater (3.5 wt.% NaCl solution) as a corrodent.

(vii) Marine foulant by mixing L DOPA (mussel protein) with 3.5 wt.% NaCl solution.

(viii) To achieve the anticorrosion and antifouling properties of the coating, the mild steel, cured epoxy, cured epoxy-chitosan nanocluster, and cured silane-modified epoxy-chitosan nanoclusters were modelled and simulated appropriately.

CHAPTER TWO

LITERATURE REVIEW

2.1 Corrosion and corrosion protection

The degradation of metals as a result of its interaction with its environment is known as corrosion. It is the oxidation of metal which is balanced by the reduction of non-metal for example, oxygen, in other to create a system of redox reaction. The oxidation of the metal which is the anodic reaction mainly occurs at the metal/environment interface while oxygen reduction which mainly occurs in solution often constitutes the cathodic reaction. Thus, the anodic and cathodic reaction together forms an electrical circuit which is completed by conduction of electron (loss of electron) from the metal substrate through the electrolyte.

In other to mitigate this reaction of metals with the environment, the metallic structure is usually isolated and prevented from coming in contact with the environment. Several techniques have been employed to achieve this, however, the use of polymeric based coating has been deemed as the most facile means of corrosion mitigation (Hsissou et al., 2020). This is because of the ability of polymer-based coatings to adsorb and form a film on metal substrates thereby isolating it from interacting with its environment. The adsorption of polymeric based coating on metal substrates are made possible because of the presence of hetero atoms such as (O, N, S, P, Si) and aromatic rings (π electrons) in polymer based coating (Dagdag et al., 2019; Hsissou et al., 2020). These hetero atoms and the aromatic rings are the main active sites of the coating which enhances the reactivity of the coating. that is, the ability of the coating to donate and/or accept electrons from the underlying metallic substrate which in turn affects the adsorption and adhesion strength of the coating and consequently the barrier performance of the coating. Thus, in other to gain insight into the anticorrosion potential performance of polymeric based coatings, there is need to understand

the reactivity and the actives sites of the coating and how these active sites will interact with the metallic substrate it intends to protect.

2.2 Assessment of anticorrosion performance of protective coatings by use of computational studies

Recently, scientists and researchers have shifted their attention towards the use of computer simulations to back-up their experimental findings. The time consumption, high cost associated with wet experiment as well as the recent development in the field of software engineering has led scientists to focus more on computer simulation.

The computer simulation technique has proved to be a useful technique which helps to elucidate the reactivity, active sites and the interaction of the coating active sites with metal substrate at the atomistic level (Dagdag et al., 2020; Uwakwe et al., 2016). This can be employed to predict the anticorrosion and antifouling properties of a coating molecules by computationally determining the active sites of inhibitor or coating molecules. These active sites are usually responsible for the inhibitor/coating-metal interaction. Properties such as the frontier molecular orbitals (FMO) as well as other quantum chemical parameters of a coating or inhibitor molecule can be analysed and could be used to assess the anticorrosion property as well as the antifouling performance of a coating or inhibitor. These properties can be calculated and analysed using the density functional theory (DFT), the molecular dynamic (MD) simulation, and Monte Carlo (MC) simulation method.

2.2.1 Anticorrosion performance evaluation by quantum chemical computation

Quantum chemical calculations are currently used by researchers to predict the behaviour of molecules in various systems. Researchers in the field of coatings and corrosion technology have successfully correlated the calculated quantum chemical parameters of a coating molecule to its anticorrosion and

antifouling performance. The frontier molecular orbitals (FMO) which are the energy of the highest occupied molecular orbital (E_{HOMO}) and the energy of the lowest unoccupied molecular orbital of a coating/inhibitor molecule are important parameters used to assess the ability of the coating/inhibitor molecule to donate and accept electrons to and from the metal surface. The E_{HOMO} and E_{LUMO} values can further be used to determine other relevant quantum chemical properties of the coating which gives insight into the reactivity of the molecule with metal substrate as well as its barrier performance.

Quantum chemical calculations via density functional theory (DFT) method are the only non-indirect source of information about the structure and energy of transition states, which, in principle, cannot be experimentally observed. Some of the properties that can be calculated with computational chemistry include equilibrium and transition-state structures, electronic excitations, reaction rates, thermochemical data.

Thus, (Cheng et al., 2020) investigated the corrosion and scale inhibitions performance of polyaspartic acid (PASP) based on the quantum chemistry calculation method. The obtained HOMO energy, the LUMO energy and the difference of the two values provided information which described the reactivity and inhibition performance of PASP molecules. In a similar way, (Nithya et al., 2016) employed quantum chemical study technique to assess the inhibition performance of a synthesized Schiff Base on the corrosion of mild steel in HCl solution. The obtained E_{HOMO} which is related to electron donating ability of inhibitor molecule showed high value of E_{HOMO}, and therefore indicates the greater tendency of inhibitor molecule to donate electron pairs to acceptor (metal substrate) with lower empty orbitals. E_{LUMO} on the other hand indicates the ability of the molecule to accept the electrons. The gap between energy of HOMO and LUMO that determines the reactivity of the molecule indicates high reactivity of

the inhibiting molecule, and thus demonstrated that the inhibitor molecules possess higher electron donating ability.

Furthermore, (Dagdag et al., 2019) studied the anticorrosion performance of two epoxy monomers namely; 2-(oxiran-2-yl-methoxy)-N, N-bis(oxiran-2-ylmethyl) aniline (AEM1) and N,N- bis(oxiran-2-yl methyl)-2-((oxiran-2-ylmethyl) thiol) aniline (AEM2) for carbon steel in 1M HCl using both experimental and computational approaches. The frontier molecular orbitals (FMO) and the quantum chemical parameters were calculated. Their findings showed that the epoxy monomer (AEM2) has a higher E_{HOMO} value of -6.156 eV while AEM1 has a lower E_{HOMO} value of -5.760 eV. However, AEM1 has a lower E_{LUMO} value of -0.474 eV. They further explained that the epoxy molecule, AEM2 with a higher E_{HOMO} value has tendency to donate electron to the empty d-orbital of iron ensuring a chemical interaction between the coating molecule and mild steel which in turn provided a better barrier performance for the mild steel. The researchers also showed that the energy gap of a molecule plays an important role in the anticorrosion performance of the molecule. They reported that AEM2 which showed better barrier performance is associated with lower energy gap. From their findings, one can conclude that coating molecules with high E_{HOMO}, low E_{LUMO} and low energy gap has the potential to provide a better barrier performance for metals.

In a similar study, (Dagdag et al., 2019) investigated the anticorrosion performance of diglycidyl ether of bisphenol A (DGEBA) cured with polyaminoamide for 2024-T3 aluminium surface in a marine environment using both experimental and computational approach. Experimental findings showed that the coating performed satisfactorily. The computational study revealed that the coating molecule is associated with high E_{HOMO} of -5.089 eV, a low E_{LUMO} of -1.289 eV and a low energy gap of 3.8 eV which were responsible for a better adsorption onto the Al substrate and consequently ensured a better anticorrosion

performance. In a separate study, (Dagdag et al., 2019) investigated the anticorrosion performance of DGEBA cured with polyaminoamide on 15CDV6 steel using both experimental and computational techniques. Again, experimental findings showed that anticorrosion performance of the coating is acceptable though there was drop in impedance after 4392 h of exposure in 3wt% NaCl. They revealed that the coating molecule can interact with mild steel via electron donation and retro-donation as it had a high E_{HOMO} of -5.13 eV, a low E_{LUMO} of -0.02 eV. However, the epoxy monomer is associated with relatively high energy gap 0f 5.15 eV which might be responsible for the coating deterioration after 4392 h of immersion in 3% NaCl.

(Dagdag et al., 2020) again investigated the anticorrosion performance of bisphenol S diglycidyl ether (DGEDDS) cured with methylene dianiline (MDA) for carbon steel in 3wt% NaCl. The DFT analysis carried out also showed that the high anticorrosion performance of the coating could be attributed to the coatings high E_{HOMO} OF -5.506 eV, low E_{LUMO} of -1.09 eV, relatively low energy gap of 4.413 eV, low electron affinity 1.09, and high ionization potential 5.506. The trend in these parameters shows the ability of the coating molecule to interact with the carbon steel via donating and accepting (retro-donation) electron from and to the carbon steel. Similarly, (Dagdag, Guo, et al., 2020) studied the barrier performance of diglycidyl ether 4,4-dihydroxydiphenyl sulfone (DGEDDS) cured with 4,4 methylene dianiline (MDA) with and without titanium oxide (TiO_2) particle for carbon steel in 3wt% NaCl using both experimental and computational techniques. Nanoparticles are usually dispersed in polymeric coating to improve their barrier performance. The nanoparticles tended to block the micro/nano pores which are usually present in cured polymeric coatings. The DFT study conducted showed that the coating interacted with the metal through electron donation. Again, they observed that the coating performance is associated with high E_{HOMO} of -4.749 eV and a low E_{LUMO} of -2.276 eV, a low

energy gap of 2.473 eV which quantified the stability and reactivity of the coating molecule.

Other parameters which can be used to determine the reactivity of coating/inhibitor molecule are the fraction of electron transferred (ΔN) and dipole moment of the coating. For a good anticorrosion coating or inhibitor, the value of ΔN is usually positive as it is expected that electrons are transferred from the coating molecule or inhibitor to the empty d-orbital if iron. The dipole moment shows the total molecular polarity at either end of the molecule. It is the product of the magnitude of charge (Q) and the distance (r) between the charges. The research group (Dagdag et al., 2020) has shown that a coating molecule with a good barrier performance is characterized by positive ΔN and a high value of dipole moment which should also be greater than the dipole moment of water (1.85 Debye). Other quantum chemical parameters can be calculated from the E_{HOMO} and E_{LUMO} using the following equations (Dagdag et al., 2020; Dagdag et al., 2019):

E_{HOMO} = energy of the highest occupied molecular orbital

E_{LUMO} = Energy of lowest unoccupied Molecular Orbital

I = ionization potential = - E_{HOMO}

A = electron affinity = - E_{LUMO}

ΔE = energy gap = E_{LUMO} - E_{HOMO}

χ = electronegativity = (I+A)/2

μ = global chemical potential = - χ

η = global hardness = (I-A)/2

σ = global softness = 1/ η

ω = electrophilicity = $\mu^2/2\eta$

ε = nucleophilicity = 1/ω

ΔN = fraction of electron transferred = $\left[\frac{\phi_{Fe}-\chi_{inh}}{2(\eta_{fe}-\eta_{inh})}\right]$

ΔG_{ads} = Gibb's free energy of adsorption = μ_{fe} - μ_{inh}

Thus, it can be concluded that a good anticorrosion coating/inhibitor is associated with high E_{HOMO}, low E_{LUMO}, low energy gap, low electron affinity, low ionization potential, high global softness, low global hardness, positive value for fraction of electron transferred, as well as high dipole moment greater than that of water (1.85 Debye).

2.2.2 Anticorrosion performance evaluation by molecular dynamics (MD) simulation

Molecular dynamics (MD) simulation is a computer simulation method used in the theoretical study of molecules, such as proteins and polymers, to analyse the physical movements of the constituent atoms and molecules. In the computer simulation, these atoms and molecules interact over time and give a sense of the dynamic evolution of the system. MD simulation mimics the changes in the structures of molecules over a given period, giving us atomic insights about the change in structure. These data help us understand functions of molecules. These simulations give us detailed information about the fluctuations and conformational changes of molecules under study. These methods are applied to thoroughly study the organization and dynamics of molecules, their complexes, and the conformational changes. Many mysteries, on the femtoseconds scale, have been revealed through the use MD simulation in the study of conformational changes. Using molecular dynamics modelling software package, interfacial features of binary or multicomponent systems can readily be obtained. MD simulations give us access to analytically unsolvable systems.

Recently, researchers in the field of corrosion technology have employed this technique to ascertain how a coating or inhibitor molecule interacts with metal surface. The orientation of coating molecule on metal surfaces, the non-covalent bond length between the atoms of the coating molecule and metal

surface and strength of the interaction between them gives an insight into the barrier performance of the coating for the metal under study. (Dagdag et al.,2019) studied the interaction of two different epoxy monomers AEM1 and AEM2 with carbon steel in other to ascertain their anticorrosion performance for the CS using the MD simulation technique. Notably, the epoxy monomers acquired a flat orientation on the CS using the heteroatoms and the aromatic rings present in the epoxy monomers. The flat orientation of the epoxy monomers on the CS (Fe110) surface could be described as the ability of the coating monomer to adsorb and form a film on the Fe (110), thus, performing as anticorrosion coating. The group also reported that AEM2 has the highest adsorption energy of -689.2 kJ/mol while AEM1 has adsorption energy of -634.0 KJ/mol. They explained that AEM2 monomer which is associated with higher adsorption energy provided a better anticorrosion performance for CS and this explanation agreed with the experimental findings. Similarly, (Dagdag et al., 2019) investigated the anticorrosion performance of DGEBA cured with polyaminoamide for aluminium in 3w% NaCl solution using the MD simulation technique. Results also showed that the epoxy monomer acquired a flat orientation on the Al surface with an adsorption energy of -252 kcal/mol with a radial distribution of 2.5A. The radial distribution function (RDF) is a useful parameter which gives insight into the type of adsorption between the coating molecule and the metal surface. (Dagdag et al., 2019) has reported that a chemical interaction is usually associated with RDF of between 1-3.5A, while physical adsorption is associated with RDF above 3.5A.

(Dagdag et al., 2019) employed the MD simulation technique to ascertain the anticorrosion performance of DGEBA-polyaminoamide monomer for 15CDV6 steel in NaCl medium. Results showed that the coating also acquired a flat orientation on the surface using the heteroatoms in the epoxy molecule. RDF analysis also revealed that chemical adsorption was the predominant type of

adsorption between the coating and steel since the RDFs of nitrogen and oxygen atoms in DGEBA-polyaminoamide with respect to steel were less than 3.5 A. The energy of adsorption was also found to be -401.39 kcal/mol. The negative sign in the energy of adsorption indicates a spontaneous interaction which also corroborated with their experimental findings. In a similar work, (Dagdag et al., 2020) investigated the anticorrosion performance of bisphenol S diglycidyl ether cured with methylene dianiline (DGEDDS-MDA) for CS in 3wt% NaCl using MD simulation technique. Results also showed that the DGEDDS-MDA adsorbed on the surface of the CS in a flat orientation using the heteroatoms (O, N, S). The adsorption energy was also found to be as high as -300.67 kJ/mol.

The anticorrosion performance of DGEDDS-MDA with and without titanium oxide (TiO_2) for CS in 3w% NaCl has also been studied by (Dagdag, Guo, et al., 2020) using MD simulation technique. Results showed that the coating adsorbed on the surface of the CS in a flat orientation with adsorption energy of -649.5 kJ/mol. However, after the addition of the TiO_2 nanocluster, the adsorption energy increased to -952 kJ/mol. These results validated the experimental findings that the addition of TiO_2 nanoparticles improved the anticorrosion performance the coating. In view of the foregoing, it can be concluded that shorter bond length between the coating molecule and the metal surface ensures increase in adsorption strength which consequently entails better anticorrosion performance of the molecule for the metal substrate under probe

2.3 Marine fouling and prevention

Marine biofouling is the undesirable settlement and growth of marine fouling organisms on artificial structures such as ship hulls, submerged oil rig facilities, offshore platforms, etc. Marine fouling may take the following forms:

Adsorption: This occurs when specific interactions between the structures and adherent particles exist. If the degree of adsorption is concentration-dependent, then concentration polarization exacerbates the amount of adsorption.

Deposition: A deposit of particles or microorganisms can grow layer by layer at the substrate surface, leading to increased hydrodynamic resistance.

Gel formation: For certain macromolecules, the level of concentration polarization may lead to gel formation in the immediate vicinity of the substrate surface.

2.3.1 Marine Biofoulers

Marine biofoulers can generally be described as organisms such as algae, bacteria, mollusk etcetera present in seawater which gets attached to the surface of marine vessels such as ship hulls, offshore oil & gas pipelines, aquaculture facilities and other structures deployed or served in the marine environment via the formation of biofilms on the surface of these structures in a process known as biofouling (Little et al., 2020).

The negative impact of biofouling cannot be overemphasized. The shipping industry is particularly severely affected. When micro/macro-organisms accumulate on the surface of the ship hulls, it accelerates the deterioration of the surface leading to increased roughness. Increase in roughness of the surface of the ship's hull consequently leads to frictional drag, increased fuel consumption, reduced ship speed with resultant economic losses. The cost of decontamination, increase in fuel consumption and cost of replacing deteriorated parts as a result of biofouling are all economic effect of biofouling (Gu et al., 2020; Urbahs et al., 2018). Increase in fuel consumption subsequently leads to increase in emission of harmful gases such carbon (IV) oxide to the environment which is attributed to be the cause of global warming and other health problems (Hakim et al., 2019). Transfer of non-indigenous micro/ macro organisms which leads to disease outbreak and damage to the environmental ecosystem has been identified as one

of the problems associated with biofouled transnational ship hulls (Georgiades et al., 2021).

2.3.2 Types and nature of marine biofoulers

More than 4000 organisms have been discovered as fouling organisms in the marine environment, either from the early stage or in its developed stage (Gu et al., 2020). Generally, fouling organisms in the marine environment can be grouped according to their sizes. Thus, in the marine environment, fouling organisms are grouped into micro-organism and macro-organism. Micro-organisms, as the name implies are minute and cannot be seen with the naked eyes. They usually play important role in the initiation of the colonization of submerged structures by biofoulers. Several micro-organisms come together to form biofilm on the surface of substrates immersed in seawater. These microorganisms in conjunction with abiotic factors such as salinity, temperature etc. enhance the corrosion of metals immersed in seawater. Micro-organisms such as bacteria, diatoms, etc. belong to this category (Georgiades et al., 2021).

Sulphate reducing bacteria, the most popular micro biofouler found in seawater have been extensively studied by researchers (Černoušek et al., 2019; Chen & Zhang, 2018; Etim et al., 2020; Liu & Cheng, 2018; Wang et al., 2021). Their growth is usually favoured in the absence of oxygen. They normally use sulphate as a terminal electron acceptor while organic compounds and hydrogen are used as electron donors as well as a source of energy. (Černoušek et al., 2019). Thus, in their favoured anoxic conditions, they gain energy by reduction of sulphate or other sulphur compounds to form hydrogen sulphide (H_2S), a corrosive substance that can accelerate the corrosion of metals. Other bacteria such as iron oxidizing bacteria (David, 2020), manganese oxidizing bacteria, sulphur oxidizing bacteria, mathenogen and acid producing bacteria (Rajala et al., 2019; Sachan et al., 2020) have been studied and found to play a major role in the corrosion of metal served in seawater.

Macro biofoulers are other set of fouling organisms found in seawater. They are larger in size and are attached to the surface of marine vessels through the biofilm already formed by the microorganisms. They are mainly responsible for the increase in ship's drag which leads to increase in fuel consumption as well as increase in the release of harmful gases to the environment (Archana & Sundaramoorthy, 2019; Urbahs et al., 2018). Organisms such as barnacles, shell fish, mollusk, and marine warms have been discovered to be marine macro biofoulers (Georgiades et al., 2021; Gu et al., 2020; Soliman & Inglis, 2018) .

2.3.3 Mechanism of attachment/colonization of substrates by marine biofoulers

Vessels submerged in seawater are usually prone to the attachment of organisms. Factors such as a search for food and nutrients, undesirable temperature, flow of water, harmful chemical compounds**,** and competition for survival encourages these organisms to move and colonize submerged structures (Procópio, 2019). Colonization of submerged surfaces by fouling organisms has been described to proceed via four steps (Chambers et al., 2006; Gu et al., 2020; Li & Ning, 2019).

The first step is the formation of biofilm on the submerged surface (Archana & Sundaramoorthy, 2019; Jia et al., 2017; Vinagre et al., 2020). After a few hours of immersion, the substrate adsorbs a biochemical conditioning biofilm (Gu et al., 2020). This biofilm is composed of proteins, polysaccharides, proteoglycans (Archana & Sundaramoorthy, 2019). Secondly, unicellular microorganisms such as bacteria and diatoms that deposit extracellular polymeric substances (EPS) which is usually sticky or slimy adheres to the substrate. The synergistic actions of the adsorbed microorganisms and the secreted extracellular polymeric substances ease the attachment of macrofoulers. Within a few days, the macrofoulers grow and provide sites for further adhesion by other micro/macroorganisms. In a few months, the substrate is completely covered by

macrofoulers because of the presence of food and nutrients. It is important to note that not all marine fouling organisms follow these steps. For instance, cyprids of barnacle can be adsorbed on submerged surfaces without biofilm (Gu et al., 2020).

2.3.4 Mechanism and kinetics of attack of marine biofoulers

The slimy layer (biofilm) formed on submerged structures after hours of immersion provides the adsorption cite for microorganisms (Dou et al., 2019). These microorganisms through their metabolic activities release or secrete extracellular polymeric substances (EPS) which are mainly made up of polysaccharides, proteins, lipids and uronic acid that condition the substrates' surfaces (Chen & Zhang, 2018). Thus, when microorganisms are adsorbed on the metal surface (biofouling), the metal starts deteriorating with time as evident by the roughening of the surface, and this phenomenon is known as microbial influenced corrosion (MIC). Generally, microbial influenced corrosion is the deterioration or degradation of metals as a result of the metabolic activities of microorganisms adhered unto the surface of the substrate. Localized form of corrosion such as pitting and crevice corrosion which is a dangerous form of corrosion because of the difficulty in early detection is usually associated with the metabolic activities of microorganisms (Zhang et al., 2021; Zhao et al., 2018).

In view of this, some studies have been conducted and therefore confirmed that biofilm and EPS play important role in the bio-corrosion of metals. (Sachan et al., 2020) has attributed the bio-corrosion of steel in the presence of pseudomonas to the reaction of iron ions with the anionic group such as OH^-, $-COO^-$, HS^- present in the EPS secreted by the bacteria. (Sachan & Singh 2018) also revealed that the concentration of EPS component of pseudomonas sp plays a significant role in the corrosion of carbon steel. They opined that the corrosion of carbon steel in the inoculated medium is accelerated via the reaction between the free Fe^{3+} in the electrolyte and EPS components.

On the other hand, according to (Lewandowski & Beyenal, 2008), biofilms adsorbed on substrates are mainly made up of four chambers, which are; the surface of attachment compartment, microorganisms and extracellular polymeric substance compartment, nutrient solution compartment and the gas phase compartment. They also explained that each chamber can be made up of different component of layer such as the bulk metal, the passive layer, biomineralized deposits on the surface as well as corrosion product. These components can be altered by the activities of microorganism in numerous ways by different microorganisms making it difficult to fully understand the mechanism and kinetics of MIC. Moreover, the biofilm provides nutrient for different microorganism, thus, supporting the growth of microbial community containing different species of microorganism with different metabolic activities and EPS component and this makes it difficult to point out a particular mechanism by which microorganisms attack metal.

CHAPTER THREE

MODEL CONSTRUCTION AND COMPUTATION

3.1 Model construction

Mild steel framework with percent (%) elemental composition given in Table 3.1 was used as a substrate. Pure iron was first imported from the materials studio software data base and other elements were incorporated into the iron via the property explorer. This was done by adjusting the percentage of pure iron and making it up by adding other elements. The build tool was used to build the mild steel frame work with a surface configuration of Fe (110).

Table 3.1: percent (%) elemental composition of mild steel

Element	Fe	C	Si	Mn	S	P	Cu	Cr
% Composition	99.24	0.14	0.03	0.32	0.05	0.20	0.01	0.01

Diglycidyl ether of bisphenol A (DGEBA) epoxy and 1,3 benzenediamide (BDA) were used as a coating resin and curing agent, respectively. Chitosan biopolymer nanocluster was used as a filler material. Two different silane molecules tetraethoxysilane & (3- aminopropyl) trimethoxy silane) were used as hydrophobic functionalizing additives. Their molecular structures are shown in Table 3.2.

These structures were sketched using the 3D atomistic visualizer of the materials studio software version 7.0. the chitosan nanocluster was also achieved using the build tool of the software. The silane modification of chitosan nanocluster was done using the method reported by (L. Wang et al., 2019). Firstly, the silane coupling agents were hydrolysed to obtain silanol. And the silanol was then manually grafted on the chitosan nanocluster by substituting it with hydrogen atoms on the surface of the chitosan nanocluster. 5% modification was

done since the chitosan nanocluster has 118 hydrogen atoms, by substituting 6 hydrogen atoms with the silanol gives 5% modification.

Table 3.2: coating materials and their molecular structures

S/N	Coating material	Molecular structure
1	Epoxy resin + benzenediamine = Epoxy coating	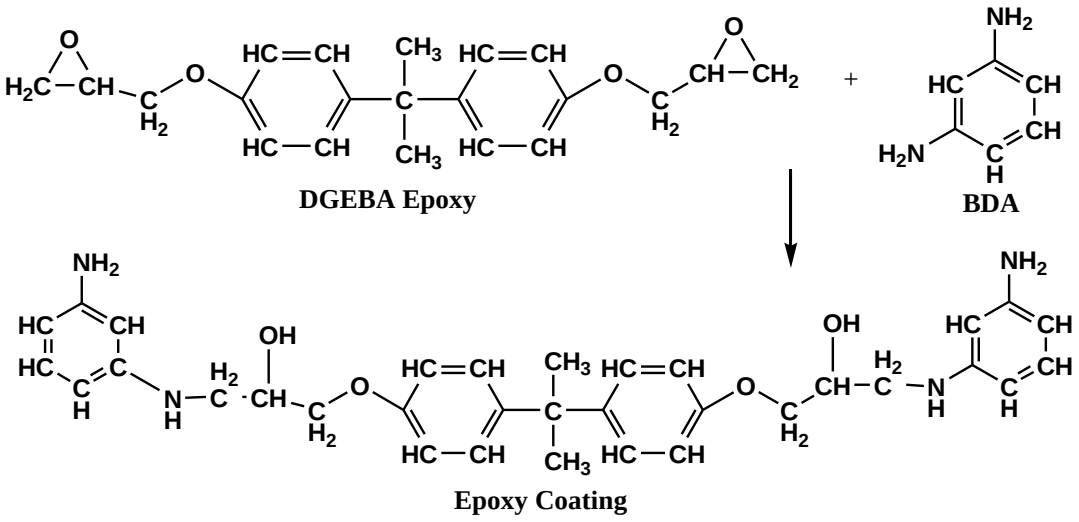 DGEBA Epoxy + BDA → Epoxy Coating
2	Chitosan oligomer	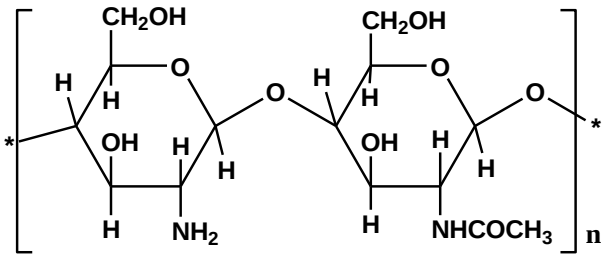
3	Tetraethoxysilane	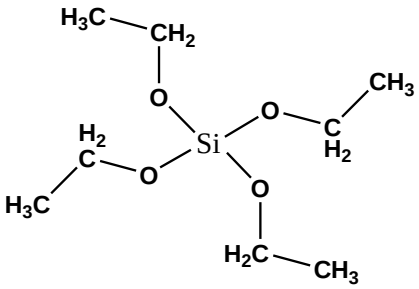
4	(3- Aminopropyl) trimethoxy silane	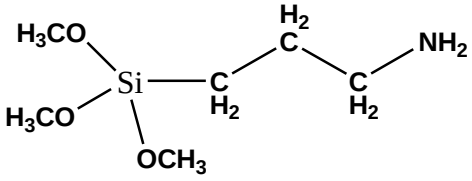

water (H_2O) and sodium chloride (NaCl) molecules were employed to simulate seawater (marine water) as corrodent using the Amorphous cell (AC) module of the software. While DOPA (3,4-dihydroxyphenylalanine) which has been recognized as a key chemical ingredient in mussel adhesion (Mian & Khan, 2017; Weinhold et al., 2006) was used for antifouling evaluation.

3.2 Computational Details

Computational method was employed in this study, and it comprises the Density Functional Theory (DFT) and Molecular Dynamics (MD) simulation techniques contained in Materials Studio software version 7.0.

3.2.1 Density Functional Theory (DFT) study.

Density functional theory (DFT) is one of the computational methods used for derivation and analysis of molecular properties. It was used to study the molecular properties and the reactive sites of the coating materials. To do this, DGEBA-BDA (epoxy resin), chitosan polymer nanocluster and silane modified chitosan polymer nanocluster were built and optimized using the forcite module at 5000 optimization steps. The method which has been described previously by (Dagdag et al., 2020) was employed. Dmol3 module of the materials studio software was used to perform DFT calculations. The calculation was done using GGA-BLYP functional, so as to achieve accuracy and reduced computational cost, DNP basis set. water with dielectric constant of 78.54 was selected as the solvent via the solvation model and COSMO. Consequently, the frontier molecular orbitals (FMO) that is, the energy of the highest occupied molecular orbital (E_{HOMO}), energy of the lowest unoccupied molecular orbital (E_{LUMO}), electrostatics and fukui functions (electrophilic and nucleophilic functions) were obtained.

Furthermore, the 'spatial descriptors' was used to ascertain the molecular area of DGEBA-BDA, chitosan nanocluster and silane modified chitosan nanocluster which gives an insight into the binding ability of the composite coating unto substrates.

Other quantum chemical parameters such as energy gap ($\Delta E = E_{LUMO} - E_{HOMO}$), ionization potential (I), electron affinity (A), electronegativity (χ), global electronic chemical potential (μ), global chemical softness (σ), global chemical hardness (η), electrophilicity and nucleophilicity were derived from the orbital energies (E_{HOMO} and E_{LUMO}) using appropriate equations (3.1 – 3.8) as previously reported in literature (Dagdag et al., 2019, Uwakwe et al., 2016). And the dipole moment was calculated using the Vamp module of the software.

$I(eV)$ = ionization potential = $- E_{HOMO}$ (3.1)

$A(eV)$ = electron affinity = $- E_{LUMO}$ (3.2)

$X(eV)$ = electronegativity = $(I+A)/2$ (3.3)

$\mu(eV)$ = global chemical potential = $- \chi$ (3.4)

$\eta(eV)$ = global hardness = $(I-A)/2$ (3.5)

$Ϭ(eV^{-1})$ = global softness = $1/\eta$ (3.6)

$GƆ(eV)$ = electrophilicity = $\mu^2/2\eta$ (3.7)

$\varepsilon(eV^{-1})$ = nucleophilicity = $1/GƆ$ (3.8)

Additionally, a few other parameters could be derived, such as fraction of electron transferred (ΔN), energy gap for back donation ($\Delta E1$) and electron donation from inhibitor HOMO to Fe LUMO ($\Delta E2$), Gibb's free energy of adsorption (ΔG_{ads})

. Thus,

$$\Delta N = \left[\frac{\phi_{Fe} - \chi_{inh}}{2(\eta_{fe} + \eta_{inh})}\right] \quad (3.9)$$

$\Delta E1 = E_{LUMO}inh - E_{HOMO}fe$ (3.10)

$\Delta E2 = E_{LUMO}fe - E_{HOMO}inh$ (3.11)

ΔG_{ads} = Gibb's free energy of adsorption = $\mu_{fe} - \mu_{inh}$ (3.12)

where theoretical E_{HOMO}fe = -5.08 eV, E_{LUMO}fe = -1.748eV.

Work function of Fe = ϕfe = 4.83eV and ηfe = 0.0ev/mol, chemical potential of iron (μ_{fe}) = -4.06eV (Dagdag et al., 2020).

3.2.2 Molecular Dynamic (MD) Simulation Study

The MD simulation technique is another method used to determine how two different molecules interact. The molecular dynamics simulation calculations were carried out to describe the interaction between the molecules of the protective coating and the metallic surface. It was performed using the quench dynamics in the forcite module contained in the materials studio software. In the study, the MD simulation was used to determine the interaction of DGEBA-BDA (epoxy coating) and mild steel, DGEBA-BDA/chitosan nanocluster and mild steel, and DGEBA-BDA/silane-modified chitosan nanocluster and mild steel in the presence of simulated seawater which served as corrodent.

The amorphous cell calculation was used to simulate salt solution by packing 500 molecules of water and 9.22 molecule of chloride ion in a cell with dimensions of a = 35A, b =35A and c = 35A. Pure iron framework was imported from materials studio data base and mild steel surface was built using the 'build' tool in the software. The whole system was assembled using the build layer tool. MD simulation was conducted in a simulation box of a = 73.35A, b = 73.35A, c = 52.309A with a periodic boundary condition.

Fe(110) was selected as the mild steel surface configuration since it is the most stable surface configuration of mild steel (Dagdag et al., 2020). The MD simulation was performed under Andersen thermostat, NVT ensemble at a temperature of 298K, with a time step of 1.0 fs and simulation time of 5 ps. The COMPASSII force field was used while non-bond interactions and van der Waals

electrostatic were set as atom-based and Ewald summation method, respectively and a cutoff radius of 15.5A was applied. Prior to the MD simulation, the whole system was optimized at 5000 optimization steps.

The radial distribution function (RDF) was used to estimate the bond length of the interacting molecules and the forcite module was also used for this calculation. The energy of adsorption was calculated after the MD simulation by first calculating the single point energy of the whole system, mild steel + salt solution, DGEBA-BDA + salt solution and the energy of solution using the forcite module and the energy of adsorption for individual coating formulation using an already established formula (Dagdag et al., 2019).

$$E_{ads} = E_{total} - (E_{surface+solution} + E_{coating+solution}) + E_{solution} \quad (3.12)$$

Where;

E_{ads} = adsorption energy, E_{total} = single point energy of the whole system, $E_{surface+solution}$ = single point energy for mild steel + 3.5wt% NaCl solution, $E_{coating+solution}$ = single point energy for DGEBA-BDA + 3.5wt% NaCl solution, and $E_{solution}$ = single point energy for 3.5wt% NaCl solution.

Furthermore, the anticorrosion potential protection efficiency of the coatings were estimated via adsorption energy values using the equation below.

$$\%P_c = \left(\frac{E_{ads}^{Mepoxy} - E_{ads}^{Uepoxy}}{E_{ads}^{Mepoxy}}\right) X\ 100 \quad (3.13)$$

Where E_{ads}^{Mepoxy} is the adsorption energy of modified epoxy coating and E_{ads}^{Uepoxy} is the adsorption energy of unmodified epoxy coating.

3.3 Anti-fouling Analysis using MD Simulation

in other to gain an insight into the anti-fouling potential of DGEBA-BDA coating as well as DGEBA-BDA reinforced with chitosan nanocluster and silane

modified chitosan nanocluster, MD simulation was used to determine the interaction of mussel protein (L-DOPA) with bare mild steel surface, DGEBA-BDA surface, DGEBA-BDA/chitosan nanocluster and DGEBA-BDA/silane modified chitosan nanocluster. L-DOPA of 5 repeat unit was constructed using the build polymer tool and the amorphous cell calculation was used to simulate the seawater by packing 500molecules of water and 9.22 molecules of Cl ion. surfaces containing 5x5 surface of DGEBA-BDA monomer, DGEBA-BDA/chitosan and DGEBA-BDA/silane modified chitosan were constructed using the build surface tool of the materials studio software version 7.0. the system was assembled using the build layer tool. MD simulation was conducted in a simulation box of a = 82.43A, b = 62.92A, c = 65.72A with a periodic boundary condition. The MD simulation was performed under Andersen thermostat, NVT ensemble with a time step of 1.0 fs and simulation time of 5 ps. The COMPASSII force field was used while non-bond interactions and van der Waals electrostatic were set as atom-based and Ewald summation method, respectively and a cutoff radius of 15.5A was applied. Prior to the MD simulation, the whole system was also optimized at 5000 optimization steps.

The adsorption energy of protein on the different substrate was calculated by modifying equation (3.12) to obtain equation 3.13 below.

$$E_{ads} = E_{total} - (E_{surface+solution} + E_{protein+solution}) + E_{solution} \qquad (3.14)$$

Where;

E_{ads} = adsorption energy, E_{total} = single point energy of the whole system, $E_{surface+solution}$ = single point energy for substrate + 3.5wt% NaCl solution, $E_{protein+solution}$ = single point energy for protein + 3.5wt% NaCl solution, and $E_{solution}$ = single point energy for 3.5wt% NaCl solution.

CHAPTER FOUR

RESULTS AND DISCUSSION

4.1 Modelling of metal framework and molecular structures of coating materials

The mild steel framework which was used as a substrate was modelled using the "build" tool contained in the 3D atomistic visualizer available in the material studio. The percent elemental composition of the mild steel is given in Table 4.1 below and the obtained mild steel framework is shown in Figure 4.1.

Table 4.1: percentage elemental composition of mild steel used in the simulation

Element	**Fe**	**C**	**Si**	**Mn**	**S**	**P**	**Cu**	**Cr**
% Composition	99.24	0.14	0.03	0.32	0.05	0.20	0.01	0.01

The obtained mild steel framework is shown in Figure 4.1.

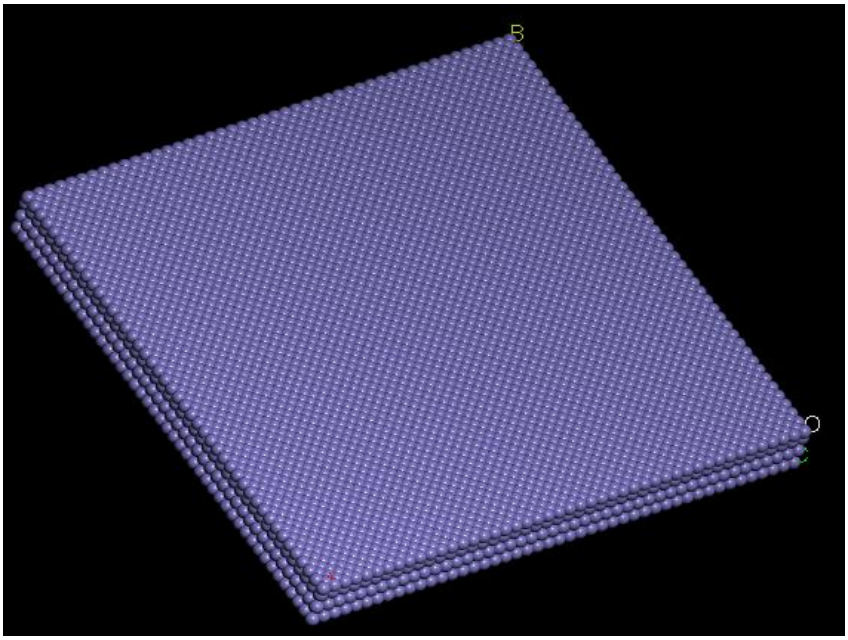

Figure 4.1: mild steel framework

Additionally, the molecular structures of the chemicals used for the preparation of coatings were modelled using the sketching tools in Materials Studio software. The diglycidyl ether of bisphenol A (DGEBA) epoxy resin and the curative, 1,3 benzenediamide (BDA) are presented in Figure 4.2.

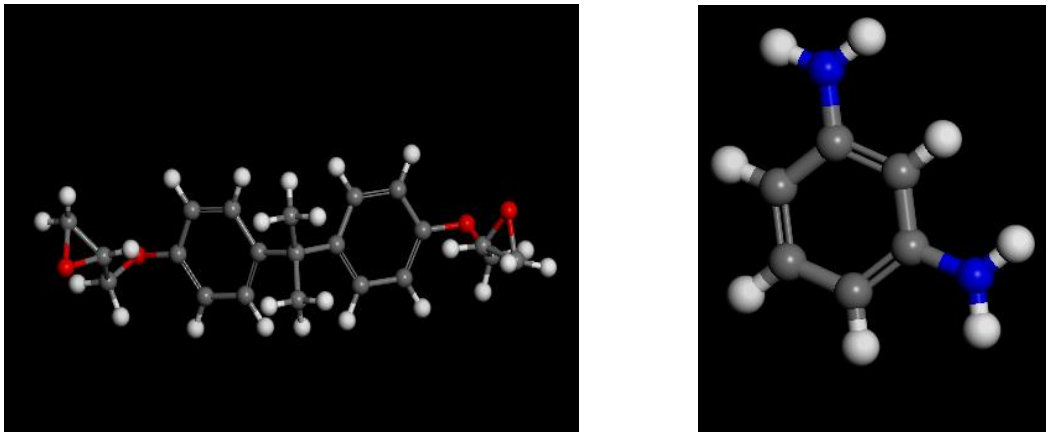

(i) (ii)

Figure 4.2: (i) diglycidyl ether of bisphenol A (DGEBA) and (ii) 1,3 benzenediamine (BDA)

The reaction of DGEBA epoxy resin and the curing agent, BDA gives an epoxy monomer. The geometry optimized molecular structure of DGEBA-BDA monomer is shown in Figure 4.3.

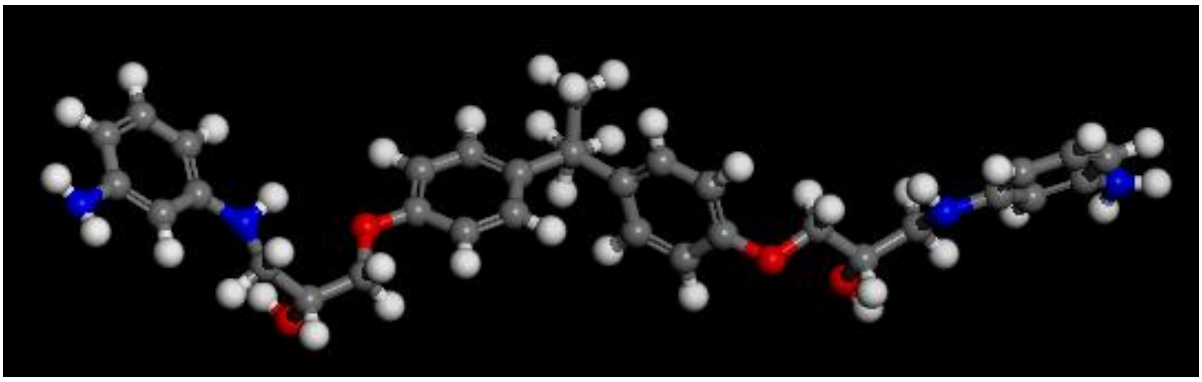

Figure 4.3: molecular structure of geometry optimized DGEBA-BDA monomer

To improve the surface functionality of the epoxy coating, chitosan biopolymer was used as a filler to plug off diffusion pathways in the epoxy coating. Thus, chitosan nanocluster was modelled by sketching chitosan monomer, and the repeat unit was increased to five (5). The obtained molecular structures are given in Figure 4.4.

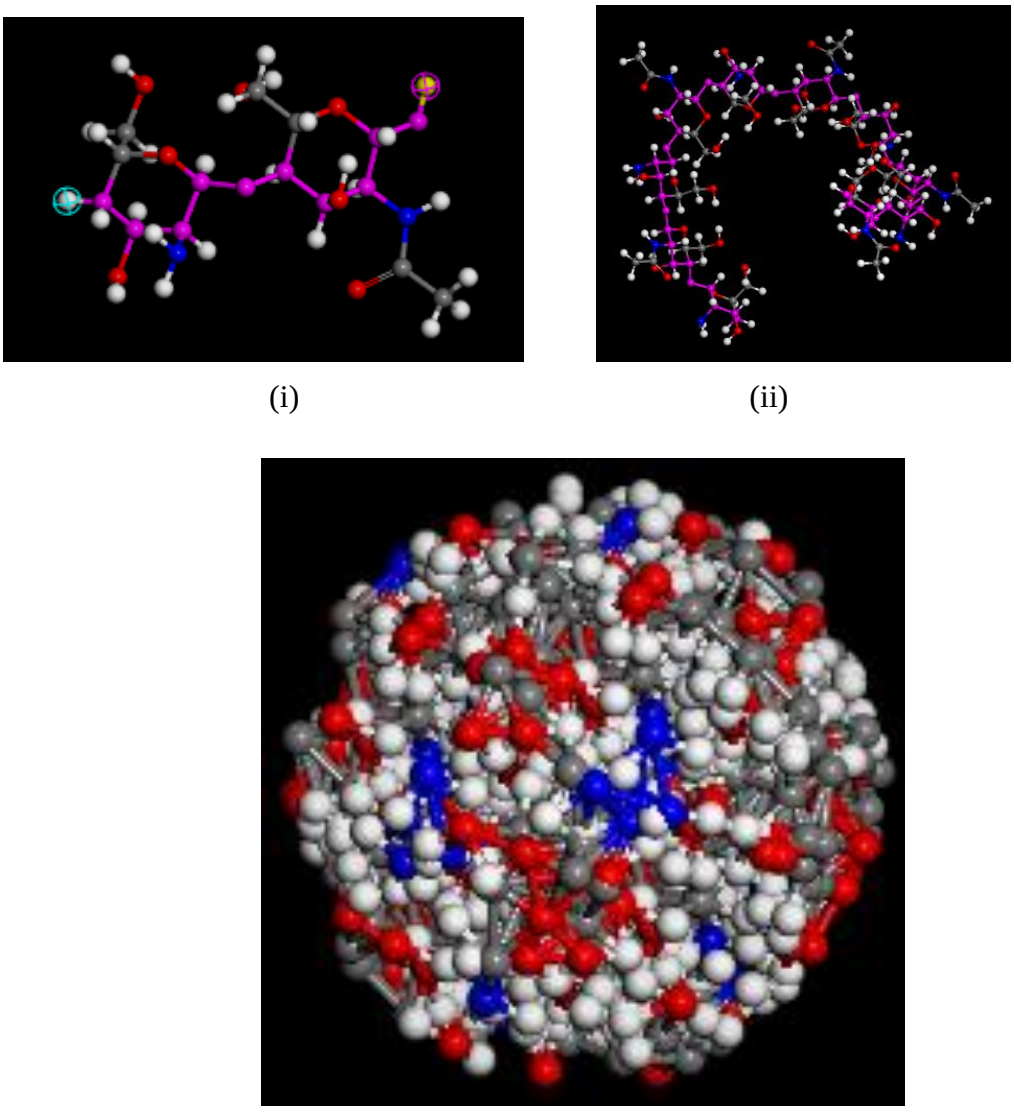

(i) (ii)

(iii)

Figure 4.4**:** Molecular structures of (i) chitosan monomer, (ii) chitosan oligomer with 5 repeat units, and (iii) chitosan nanocluster.

Besides, the chitosan nanostructured epoxy coating was further modified with silane additives to improve its surface properties by way of enhancing the

hydrophobicity. The geometry optimized molecular structures of the silane additives are presented in Figure 4.5.

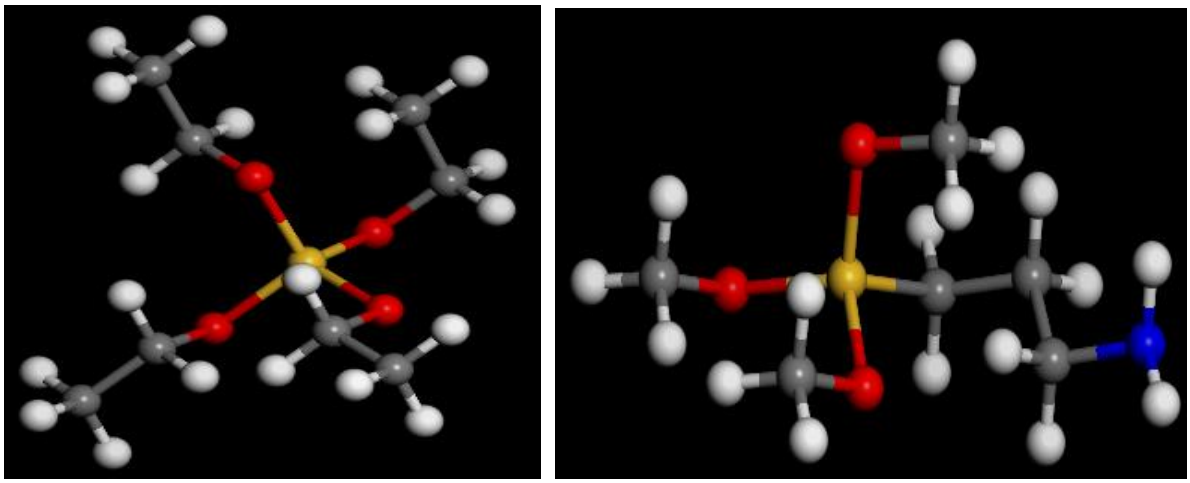

(i) (ii)

Figure 4.5: (i) Tetraethoxysilane, and (ii) (3- Aminopropyl) trimethoxy silane

For anti-corrosion simulation, seawater is used. It was simulated by mixing adequate proportion of NaCl in a given amount of water. For NaCl-water solution, the main drivers of corrosion are water and chloride ion. Thus, optimized molecular structures of water and chloride ion are presented in Figure 4.6.

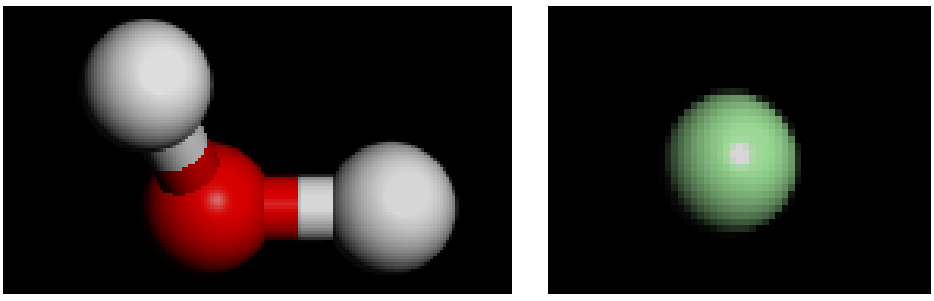

Figure 4.6**:** Optimized molecular structures of (i) water and (ii) chloride ion.

For anti-fouling experiment, levodopa (L-DOPA) which is a major amino acid component of mussel protein found in both salt and fresh water that facilitates wet adhesion to substrates was used. The molecular structures of L-DOPA monomer and L-DOPA with five (5) repeat units are given in Figure 4.7.

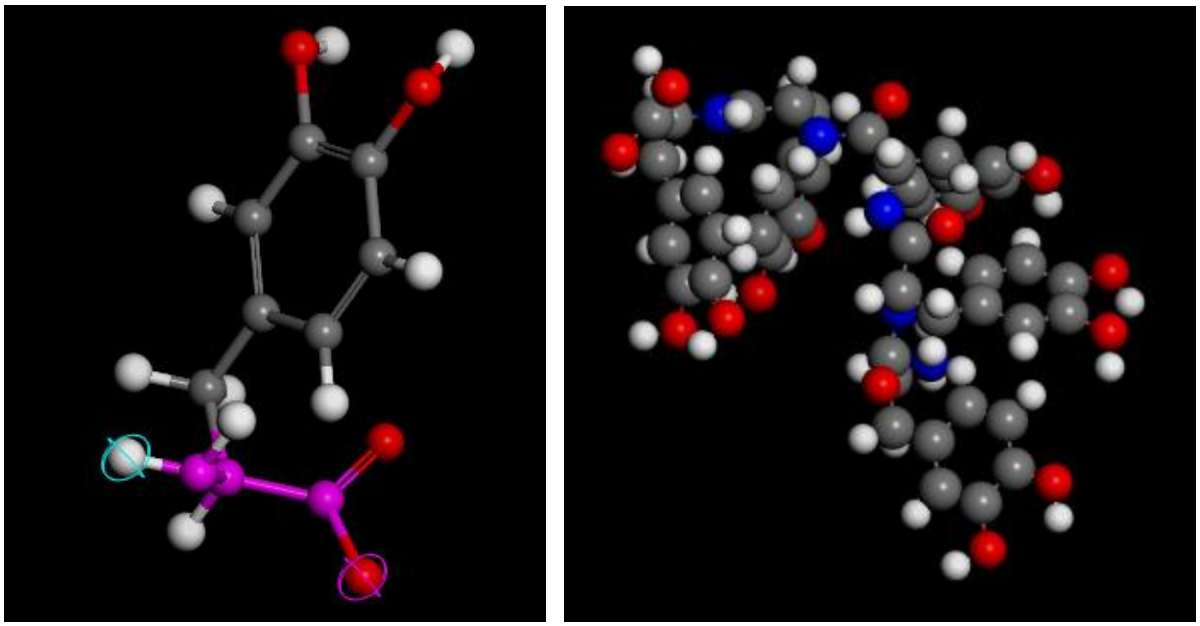

(i) (ii)

Figure 4.7**:** Molecular structures of (i) L-DOPA monomer and (ii) L-DOPA with five (5) repeat units

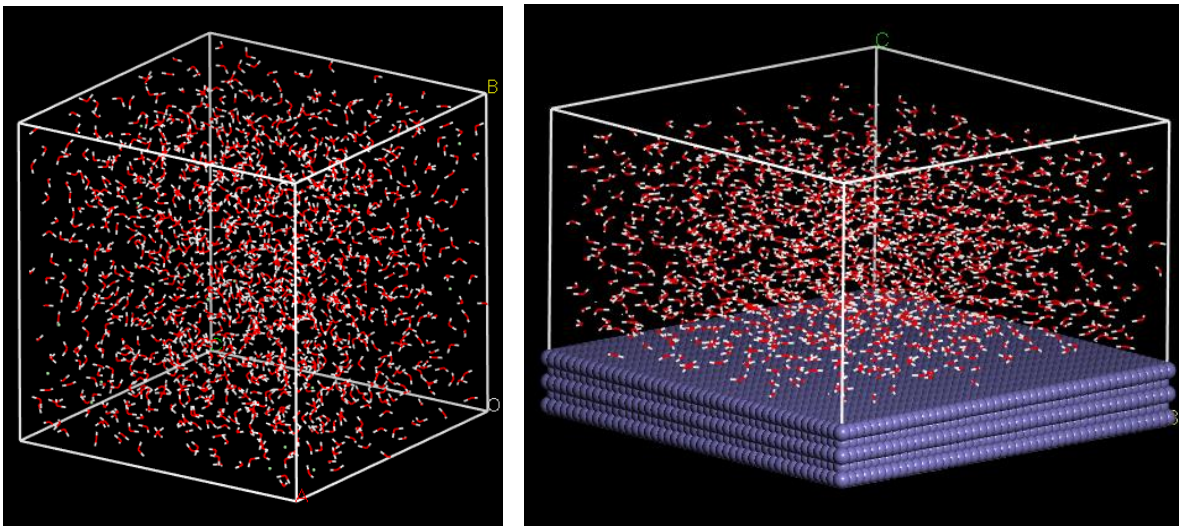

(i) (ii)

Figure 4.8 (i). Salt solution: 96.5% water, 3.5% chlorine & (ii) Mild steel immersed in salt solution, Water & chloride ion

4.2 Anti-Corrosion Properties Analyses by Density Functional Theory (DFT) study

The optimized highest occupied molecular orbital (HOMO), lowest unoccupied molecular orbital (LUMO) and electrostatic potential (ESP) structures of the DGEBA-BDA are presented in Figure 4.9. Other quantum chemical parameters for DGEBA-BDA were also determined. The obtained parameters are given in Table 4.2. in addition, the HOMO and the LUMO orbitals for chitosan, TEOS-chitosan and APTES-chitosan were obtained and are presented in figures 4.10, 4.11 and 4.12 respectively. The quantum chemical parameters for chitosan, TEOS-chitosan and APTES-chitosan were calculated and are presented in Table 4.3.

Furthermore, the molecular area which reveals the van der Waals area of a molecule. And consequently, determines the extent to which a molecule exposes itself to the external environment were also determine for the DGEBA-BDA, chitosan as well as silane modified chitosan and the results are shown in Table 4.4.

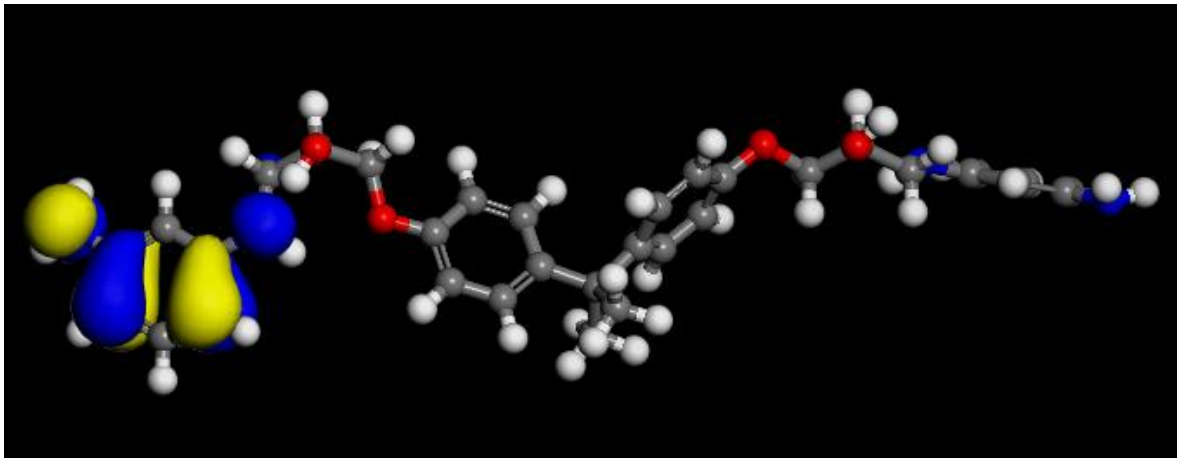

(i)

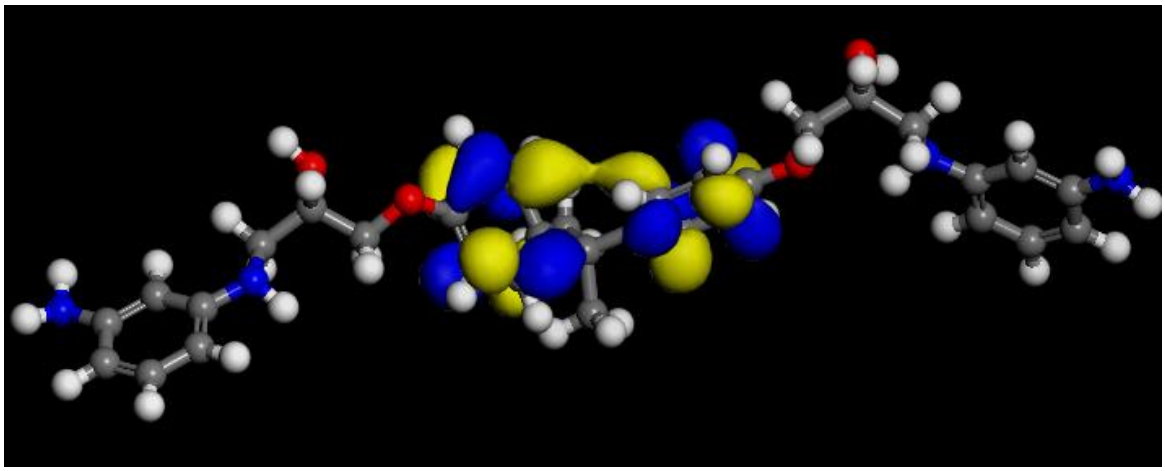

(ii)

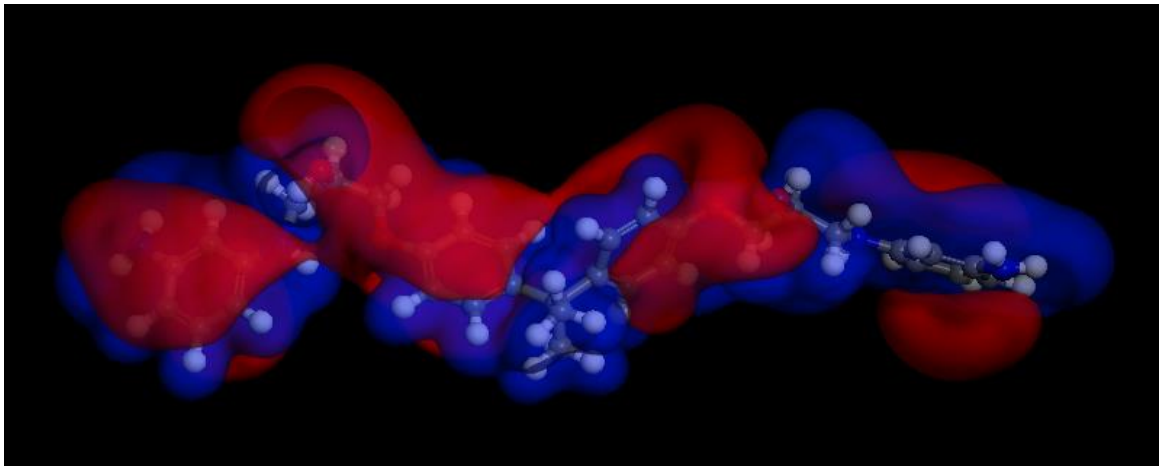

(iii)

Figure 4.9: (i) HOMO, (ii) LUMO, and (iii) ESP of optimized DGEBA-BDA.

Table 4.2: Quantum chemical parameters of DGEBA-BDA

E_{HOMO}	E_{LUMO}	ΔE	I	A	χ	μ	η	Ϭ	Ꞷ	ε	ΔN	$\Delta E1$	ΔE2
-4.706	-1.018	3.688	4.706	1.018	2.862	-2.862	1.844	0.54	2.22	0.45	0.533	4.062	2.958

Dipole moment	ΔG_{ads}
4.654 debye	-115.595kj/mol

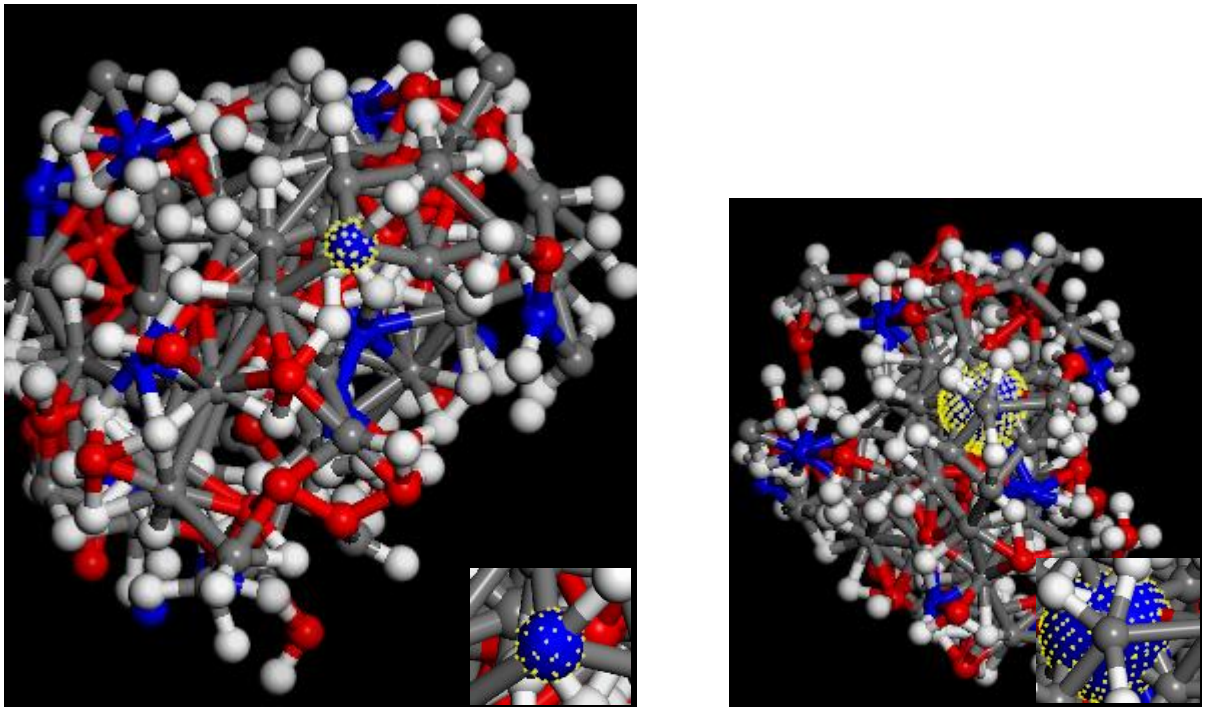

(i) (ii)

Figure 4.10: (i) HOMO, (ii) LUMO orbitals of optimized chitosan nanocluster

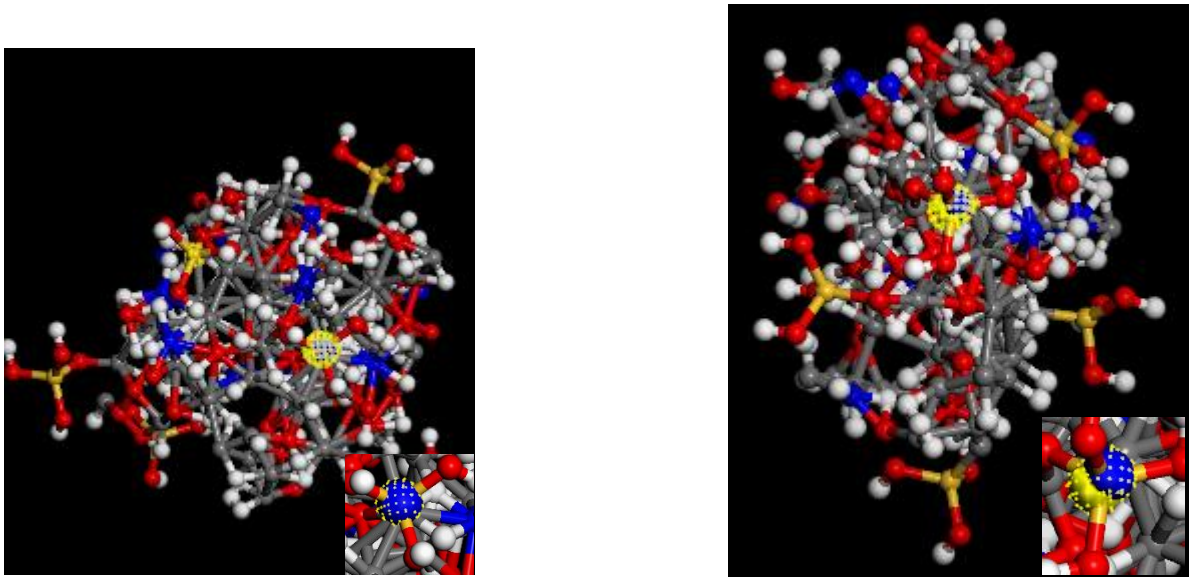

(i) (ii)

Figure 4.11: (i) HOMO, (ii) LUMO orbitals of optimized TEOS-chitosan nanocluster

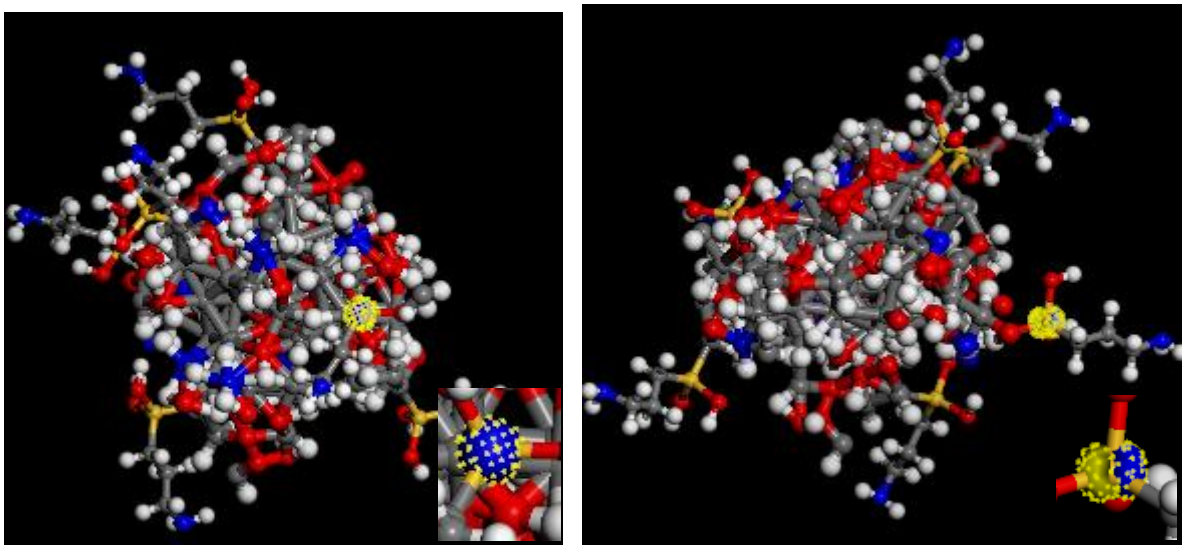

(i) (ii)

Figure 4.12: (i) HOMO, (ii) LUMO orbitals of optimized APTES-chitosan nanocluster

Table 4.3: Quantum chemical parameters for chitosan, TEOS-chitosan and APTES-chitosan nanocluster

nanocluster	E_{HOMO}	E_{LUMO}	ΔE	I	A	χ
chitosan	-322.710	-286.828	35.828	322.710	286.828	304.769
TEOS/chitosan	-262.530	-229.425	33.105	262.530	229.425	245.977
APTES/chitosan	-264.864	-232.438	32.426	264.864	232.438	248.651

nanocluster	μ	η	ϭ	ϢϢ	ε
chitosan	-304.769	17.941	0.0557	2588.59	0.000386
TEOS/chitosan	-245.977	16.555	0.0604	1827.93	0.000547
APTES/chitosan	-248.651	16.213	0.0616	1906.72	0.000524

Table 4.4: Summary of the molecular area for epoxy, chitosan nanocluster and silane modified chitosan nanocluster

Monomer/nanocluster	Molecular area (A^2)
DGEBA-BDA	641.004
Chitosan nanocluster	1129.179
TEOS-chitosan	1502.724
APTES-chitosan	1923.005

4.2.1 HOMO and LUMO Orbitals and Quantum Chemical Parameters Results

The HOMO and LUMO values of a molecule are important parameters in determining the reactivity of a molecule as well as in predicting the anticorrosion performance of such molecule. It is well known that the HOMO region is electron-rich region which is willing to donate electron to the empty d-orbital of metal. Close examination of Figure 4.9(i) shows that HOMO region is located mainly at the benzenediamine region which contains aromatic ring, amino group and secondary amine.

The LUMO region (see Figure 4.9 (ii)) is electron-deficient region which is responsible for back donation or retro donation. Simply put, it is the region of the molecule that accepts electron from metal during coating-metal interaction. The LUMO for DGEBA-BDA is located at the central part of the DGEBA-BDA epoxy coating molecule containing bisphenol A molecule.

Reports have shown that coating molecules with high HOMO value and low LUMO value can interact and adsorb on mild steel surface and perform as good anticorrosion coating (Dagdag et al., 2020; Dagdag et al., 2020). Table 4.2 reveals that DFT calculation of DGEBA-BDA epoxy coating molecules presents high HOMO value of -4.706 eV and relatively low LUMO value of -1.018 eV. The energy gap, ΔE obtained for DGEBA-BDA is 3.688 eV. The low value of ΔE indicates that the coating molecules is less stable and can easily bond with metal substrates. Thus, adequate protection to the metal surface is assured. The observed results clearly indicate that DGEBA-BDA has strong ability to interact with mild steel surface via electron donation as well as back donation. This is in agreement with other studies reported elsewhere (Uwakwe et al., 2016; Dagdag et al., 2020).

Fraction of electron transferred (ΔN) is another important parameter that can be used to assess anticorrosion coating capability of molecules. (Dagdag et

al., 2020) stated that electrons will be transferred from the HOMO of a coating molecule to the LUMO (empty d-orbital) of mild steel if ΔN is less than 3.6 and also has positive value, while there will be a retro donation if ΔN is negative. Table 4.1 shows that the obtained value of ΔN for DGEBA-BDA is 0.533 which is positive and less than 3.6. This finding indicates that good interaction of DGEBA-BDA coating molecules with mild steel surface is because electrons were readily transferred from the DGEBA-BDA HOMO region to the empty d-orbital of mild steel, confirming the anti-corrosion property of DGEBA-BDA coating molecules.

ΔE1 and ΔE2 represent the energy gap for retro donation (donation of electron from HOMO of iron to the LUMO of coating molecule) and donation of electron from the HOMO of the coating molecule to the empty d-orbital (LUMO) of iron, respectively. It has been reported that for good anti-corrosion coating, electrons are preferably transferred from the HOMO of the coating molecule to the LUMO (empty d-orbital) of iron (Dagdag et al., 2020). Thus, Table 4.1 shows that $\Delta E1 > \Delta E2$, which is an indication that for the DGEBA-BDA-Fe interaction, electrons are preferentially donated from the HOMO of DGEBA-BDA to the empty d-orbital of Fe. This, also validates our results with ΔN, confirming that DGEBA-BDA coating will provide adequate protection to mild steel.

Furthermore, the Gibb's free energy (ΔG_{ads}) of adsorption and dipole moment of DGEBA-BDA which can be used to estimate the type of adsorption between DGEBA-BDA monomer and mild steel were obtained. A physical interaction between mild steel and inhibitor molecule is expected when the Gibb's free energy is between 0 to -40kj/mol while -80 to -400kj/mol marks chemical adsorption (Dagdag, Guo, et al., 2020). Herein, the ΔG_{ads} is found to be -115.595kj/mol which indicates that the adsorption between DGEBA-BDA and mild steel will be spontaneous chemisorption. The dipole moment of DGEBA-BDA was also found to be 4.654debye which is greater than the dipole moment

of water (1.85debye) which is an indication that DGEBA-BDA will preferentially adsorb on mild steel surface in the presence of water.

On the other hand, the HOMO and LUMO orbitals of chitosan, TEOS-chitosan and APTES-chitosan are shown in figures 4.10, 4.11 and 4.12 respectively. The result revealed that the HOMO and LUMO orbitals of chitosan is mainly located at the $-NH_2$ and $-NHCOCH_3$ moiety respectively (see figure 4.10(i)&(ii)). However, after modifying with silane (TEOS & APTES) the HOMO and the LUMO orbitals were observed at the silane (Si) moiety for both TEOS and APTES modified chitosan nanocluster. (See figures 4.11 & 4.12).

Chitosan nanocluster and silane modified chitosan nanocluster are associated with high HOMO value and relatively low LUMO value. See Table 4.3. it can be seen that the silane modified chitosan nanocluster is associated with low energy gap with APTES-chitosan nanocluster having the lowest energy gap. In addition, the ionization potential of silane modified chitosan is observed to be lower than the unsilanized chitosan nanocluster. This indicates that silane modified chitosan nanocluster is more reactive than the unsilanized chitosan nanocluster and consequently has the potential to adsorb better on mild steel surface (Uwakwe et al., 2016).

Furthermore, silane modified chitosan is associated with higher molecular area compared to unsilanized chitosan nanocluster see Table 4.4. this parameter has been described as an important parameter which describes the binding ability of a molecule (Martinez, 2002). This parameter helps to elucidate the van der Waals area of a molecule which in turn influences the extent to which a molecule exposes itself to the external environment such as mild steel surface. We observed that silane modified chitosan nanocluster has larger molecular area compared to unsilanized chitosan nanocluster with APTES-chitosan having the largest molecular area, thus, having the potential to adsorb better on substrates.

4.2.2. Electrostatic potential (ESP) results

Figure 4.9(iii) shows the electrostatic potential (ESP) map or distribution of electrons on the DGEBA-BDA molecule. ESP map gives an insight into a better understanding of the reactive sites or region of the coating molecules. The region in red colour indicates the electron rich region which are preferred sites for electrophilic attack while the blue area shows the electron deficient area which are also susceptible to nucleophilic attack. The region in red colour is mainly distributed on extreme of the coating molecules which also coincides with the location of the HOMO. Thus, we can say that this region is the site for electrophilic attack. Meanwhile, the blue-coloured region is electron deficient region. This region is also seen around the central part of the cured epoxy coating molecules, which aligns with the LUMO region. This region is susceptible to nucleophilic attack as they are willing to accept electron from the mild steel. Thus, these sites are utilized by the coating molecule for attachment unto the mild steel by accepting and donating electron from the mild steel.

4.2.3 Fukui indices results for DGEBA-BDA, chitosan and silane modified chitosan

During coating molecule-metal interaction, electron donation usually takes place from the HOMO of coating molecule to the vacant d orbital of metal or from metal to the LUMO of the inhibitor (retro donation). This HOMO and LUMO sites are usually the reactive sites of a coating molecule. The Fukui functions which are derived from DFT studies have proven to be a great tool in the determination of these active sites (Dagdag et al., 2020). Figure 4.13 shows the Fukui electrophilic and nucleophilic maps, respectively.

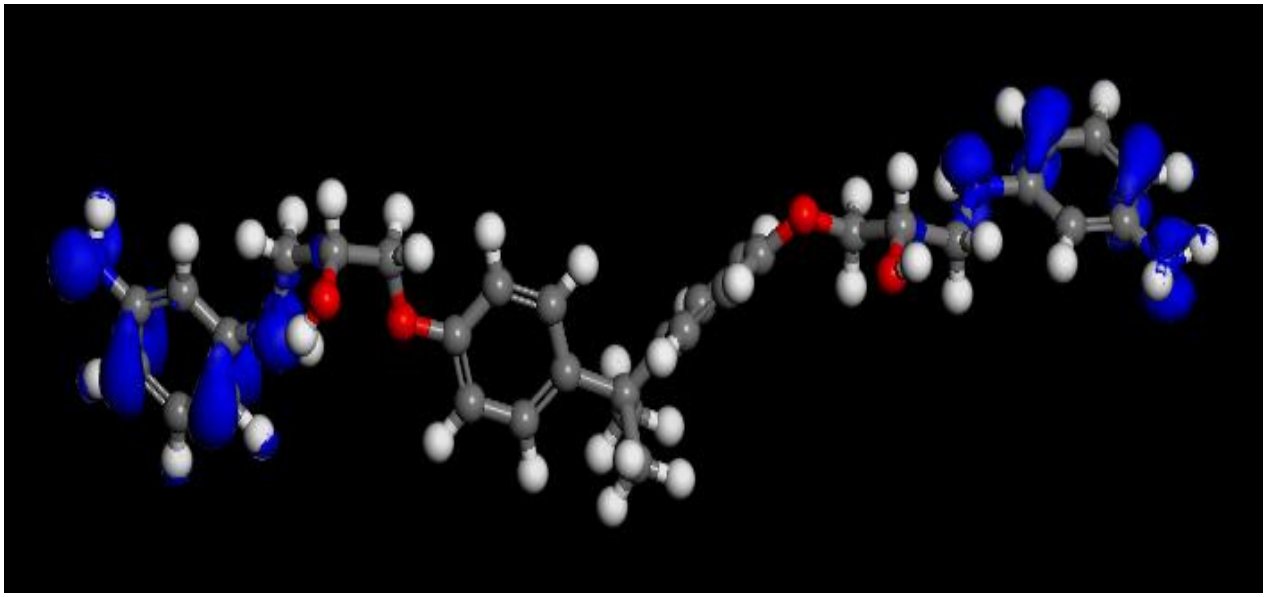

(i)

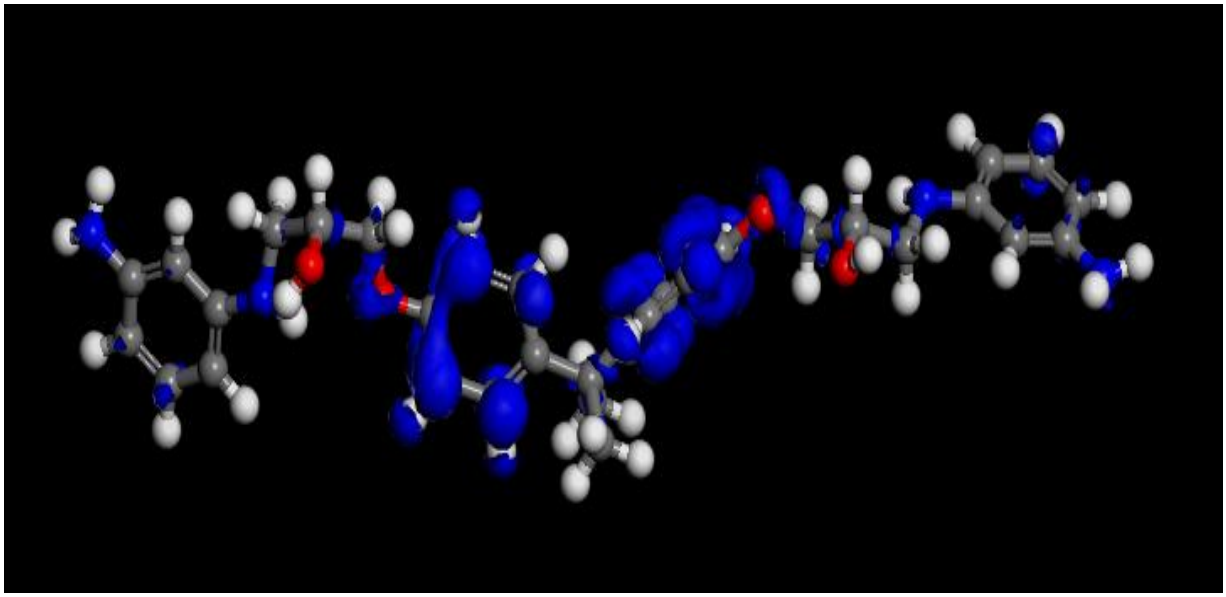

(ii)

Figure 4.13: Fukui functions for (i) electrophilic and (ii) nucleophilic maps

The electrophilic region is the electron-rich area which is susceptible to electrophilic attack, and it is located at the extreme part of the DGEBA-BDA coating molecule which is mainly made up of benzenediamine. The nucleophilic area is electron-deficient area which is susceptible to nucleophilic attack. This

area is also located at the central part of the DGEBA-BDA molecule where we have the bisphenol A. These results are also in agreement with those of HOMO and LUMO maps.

The optimized structure of DGEBA-BDA monomer showing numbering of atoms is presented in Figure 4.10.

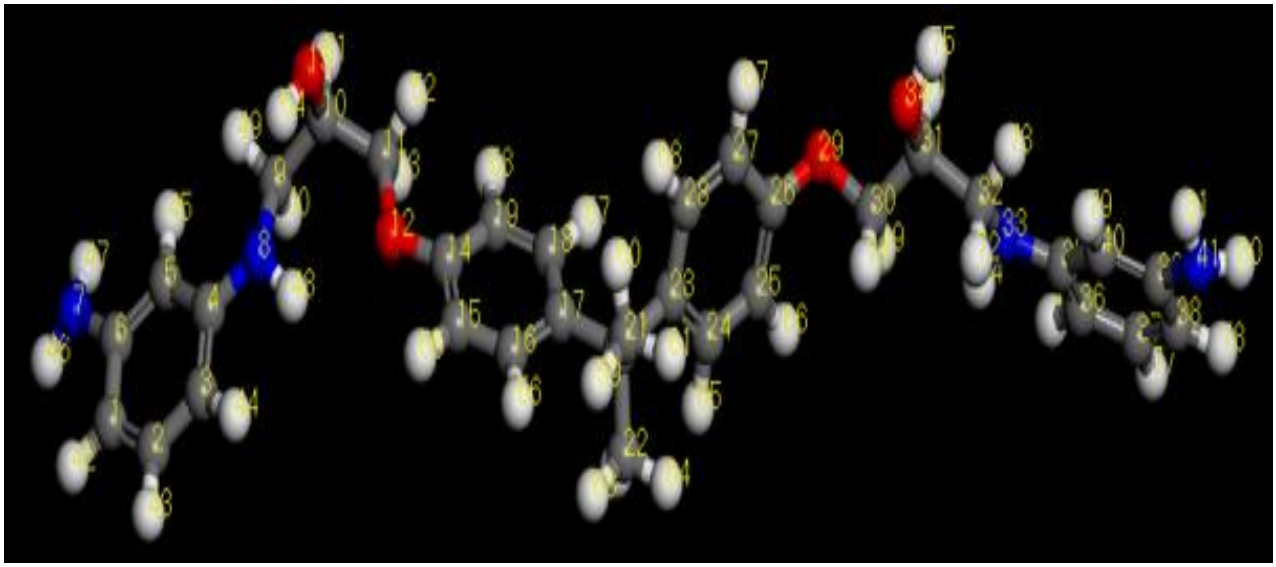

Figure 4.14: The optimized structure of DGEBA-BDA coating showing numbering of atom.

Furthermore, the graphical representation of the highest and lowest dual descriptor, $f^2(r)$ based on calculated Fukui function are presented in figure 4.15.

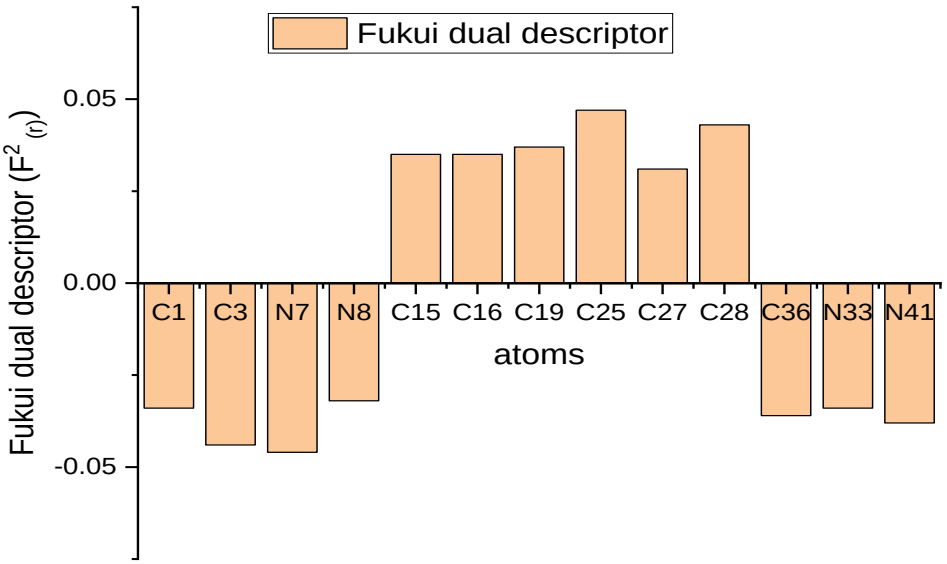

Figure 4.15: The graphical representation of the highest and lowest values of the dual descriptor ($f^2(r)$) based on calculated Fukui function for DGEBA-BDA coating.

Thus, the values of the Fukui electrophilic $f^+(r)$, nucleophilic $f^-(r)$ and Fukui dual descriptor $f^2(r)$ values for the individual atoms in the DGEBA-BDA coating molecules are given in Table 4.5.

Table 4.5: Fukui electrophilic ($F^{-}(k)$), nucleophilic ($(f^{+}(k))$) and dual Fukui descriptor ($(F^{2}(r))$) values for DGEBA-BDA

Atoms	$F^{+}(r)$	$(F^{-}(r))$	$F^{2}(r)$	**Atoms**	$F^{+}(r)$	$F^{-}(r)$	$F^{2}(r)$
C1	0.007	0.041	-0.034	C22	-0.014	0.001	-0.015
C2	0.009	0.005	0.004	C23	-0.004	0.000	-0.004
C3	0.001	0.045	-0.044	C24	0.027	0.001	0.026
C4	0.001	0.011	-0.010	C25	0.047	0.000	0.047
C5	0.008	0.017	-0.009	C26	0.023	-0.002	0.025
C6	0.004	0.010	-0.006	C27	0.032	0.001	0.031
N7	0.007	0.053	-0.046	C28	0.043	0.000	0.043
N8	-0.001	0.031	-0.032	O29	0.019	0.002	0.017
C9	-0.004	-0.017	0.013	C30	-0.016	0.001	-0.017
C10	-0.003	-0.006	0.003	C31	-0.002	-0.002	0.000
C11	-0.018	-0.003	-0.015	C32	-0.004	-0.015	0.011
O12	0.018	-0.010	0.028	N33	-0.001	0.033	-0.034
O13	0.005	0.015	-0.010	O34	-0.006	0.009	-0.015
C14	0.016	-0.002	0.018	C35	0.002	0.009	-0.007
C15	0.036	0.001	0.035	C36	0.003	0.039	-0.036
C16	0.037	0.002	0.035	C37	0.012	0.004	0.008
C17	-0.003	0.003	-0.006	C38	0.007	0.036	-0.029
C18	0.029	0.002	0.027	C39	0.005	0.009	-0.004
C19	0.038	0.001	0.037	C40	0.009	0.014	-0.005
C20	-0.012	-0.002	-0.010	N41	0.006	0.044	-0.038
C21	-0.014	-0.002	-0.012				

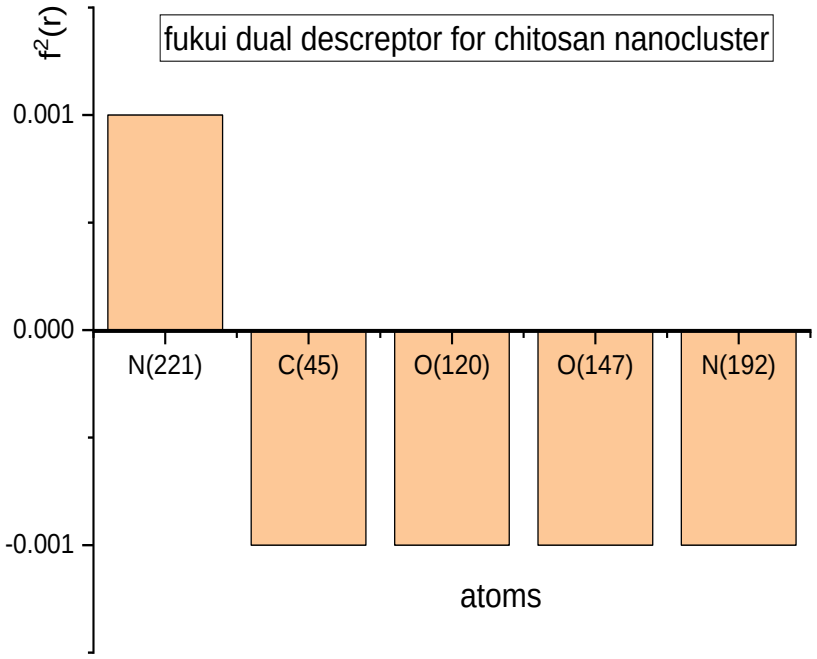

Figure 4.16: The graphical representation of the highest and lowest values of the dual descriptor (f2(r)) based on calculated Fukui function for chitosan nanocluster

Table 4.6: Fukui electrophilic (F+(k)), nucleophilic ((F-(k))) and dual Fukui descriptor ((F2(r))) values for chitosan nanocluster

atoms	$F^{+}(k)$	$f^{-}(k)$	$F^{2}(r)$
N(221)	0.003	0.002	0.001
C(45)	0.009	0.01	-0.001
O(120)	0.001	0.002	-0.001
O(147)	0.003	0.004	-0.001
N(192)	0.001	0.002	-0.001

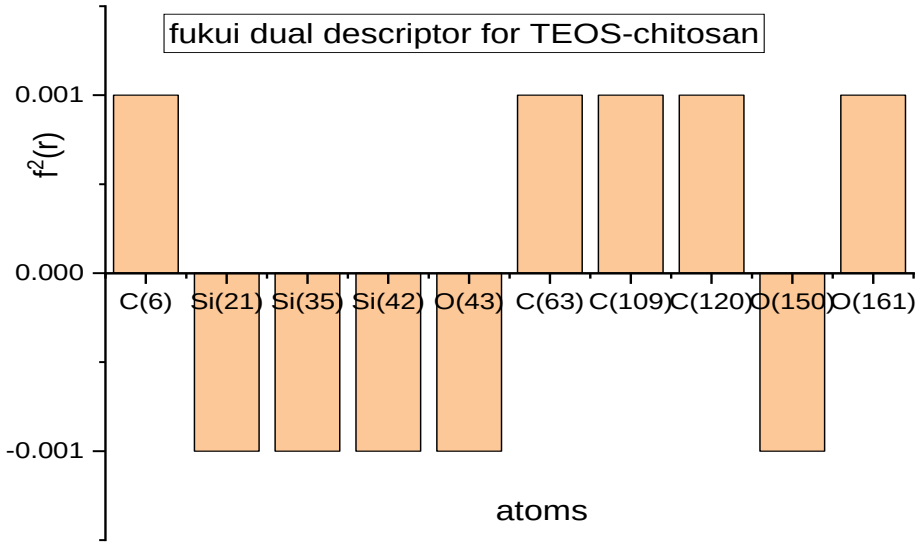

Figure 4.17: The graphical representation of the highest and lowest values of the dual descriptor (f2(r)) based on calculated Fukui function for TEOS- chitosan nanocluster

Table 4.7: Fukui electrophilic (F^-(k)), nucleophilic ((F^+(k))) and dual Fukui descriptor ((F2(r))) values for TEOS- chitosan nanocluster

atoms	F^-(k)	F^+(k)	F^2(r)
C(6)	0.003	0.002	0.001
Si(21)	0.014	0.015	-0.001
Si(35)	0.013	0.014	-0.001
Si(42)	0.008	0.009	-0.001
O(43)	0.011	0.012	-0.001
C(63)	0.006	0.005	0.001
C(88)	0.005	0.006	-0.001
C(109)	0.005	0.004	0.001
C(120)	0.01	0.009	0.001
O(150)	0.004	0.005	-0.001
O(161)	0.002	0.001	0.001
H(211)	0	0.001	-0.001
C(225)	0.006	0.007	-0.001
H(249)	0	0.001	-0.001

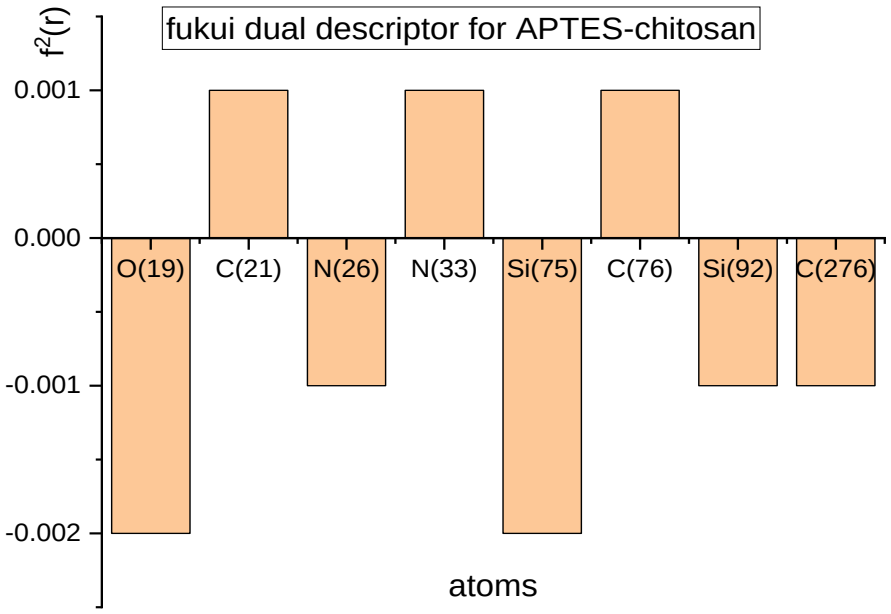

Figure 4.18: The graphical representation of the highest and lowest values of the dual descriptor (f2(r)) based on calculated Fukui function for APTES- chitosan nanocluster

Table 4.8: Fukui electrophilic (F-(k)), nucleophilic ((F^{+}(k))) and dual Fukui descriptor ((F^{2}(r))) values for APTES- chitosan nanocluster

atoms	F^{+}(k)	f^{-}(k)	F^{2}(r)
O(19)	0.004	0.006	-0.002
C(21)	0.005	0.004	0.001
N(26)	0.006	0.007	-0.001
N(33)	0.005	0.004	0.001
Si(75)	0.004	0.006	-0.002
C(76)	0.003	0.002	0.001
Si(92)	0.007	0.008	-0.001
C(276)	0.001	0.002	-0.001

To better understand the relevance of these Fukui parameters, (Dagdag et al., 2020) has shown that the Fukui dual descriptor function $F^{2}(r)$ which is given by $f^{+}(k) - f^{-}(k)$ is a better way of analysing the active sites of the molecule. Hence, atoms with $F^{2}(r) > 0$ are electron deficient atoms which are sites for nucleophilic attack. They are sites that accept electron from the metal substrate during coating-metal interaction while atoms with $F^{2}(r) < 0$ are electron rich atoms. These atoms are sites for electrophilic attack. They donate electron to the empty d-orbital of iron during coating molecules-metal interaction.

A proper study of Table 4.5 and Figure 4.15 shows that atoms with $F^{2}(r) > 0$ follows the trend, C25 > C28 > C19 > C15 & C16 > C27 which form the aromatic ring located at central part of the DGEBA-BDA coating. These atoms accept electrons from metal substrates during coating molecule-metal interaction and are sites for nucleophilic attack while atoms with $F^{2}(r) < 0$ follows the trend;

N7 > C3 > N41 > C36 > N33 & C1 > C27. These atoms are electron-rich atoms located at the benzenediamine region. They usually donate electrons to the vacant d-orbital of metals during coating molecule-metal interaction. Thus, they are preferred sites for electrophilic attack. These results are quite in agreement with the HOMO and LUMO results.

On the other hand, the F+(k)), (F-(k) & $F^2(r)$ for chitosan nanocluster are presented in figure 4.16 and Table 4.6. it is clear that the electron deficient region ($F^2(r) > 0$) is at N(221) while the electron rich region ($F^2(r) < 0$) are atoms: C(45), O(120), O(147), N(192) which are responsible for electron donation during interaction with mild steel. After TEOS modification, we observed the electron deficient atoms that is; $F^2(r) > 0$ to be atoms: C(6), C(63), C(109), C(120) and O(161) while the electron rich region ($F^2(r) < 0$) are atoms: Si(21), Si(35), Si(42) and O(43) (see Table 4.7 and figure 4.17). furthermore, the electron deficient region ($F^2(r) > 0$) is seen at atoms: C(21), N(33) & C(78) while the electron region is seen at atoms: Si(75), O(19), N(28), Si(92) & C(276) when modified with APTES. This shows that treating chitosan with silane coupling agents can improve its reactivity as well as its active sites through with it can interact with mild steel surfaces.

4.3 Anti-Corrosion Potential evaluation by Molecular Dynamic (MD) Simulation

Molecular dynamic simulation is a useful computer simulation technique used to determine how different molecules interact and the type of interaction existing between the interacting molecules. This method has been employed by researchers in the field of corrosion and coating technology to probe the anticorrosion performance of novel coatings (Dagdag et al., 2019; Uwakwe et al., 2016).

Herein, the MD simulation was used to determine the interaction between mild steel and DGEBA-BDA coating. The orientation of DGEBA-BDA coating

molecules on mild steel surface, the bond length between the coating atoms and the mild steel surface, as well as the adsorption energy of the interaction was determined and used to assess the anticorrosion performance of DGEBA-BDA coating on mild steel. Furthermore, the MD simulation was also used to determine effect of chitosan nanocluster and silane-modified chitosan nanocluster on the adsorption and anticorrosion performance of DGEBA-BDA coating.

4.3.1 Adsorption of epoxy coating (DGEBA-BDA) monomer on mild steel surface

The adsorption of DGEBA-BDA, DGEBA-BDA/chitosan nanocluster and DGEBA-BDA/silane modified chitosan nanocluster on mild steel surface in the presence of 3.5 wt% NaCl solution was studied using the MD simulation. Figure 4.19 shows the interaction of DGEBA-BDA coating monomer with mild steel surface in the presence of 3.5 wt.% NaCl solution. It can be seen that the monomer adsorbs on mild steel surface in a flat orientation using its active sites. that is; the heteroatoms (O, N) as well as the aromatic rings. The flat orientation of the monomer on mild steel surface can be attributed to large molecular area of the monomer(Martinez, 2002) and this shows that the monomer can spread out on mild steel surface and form a film (Hsissou et al., 2020).

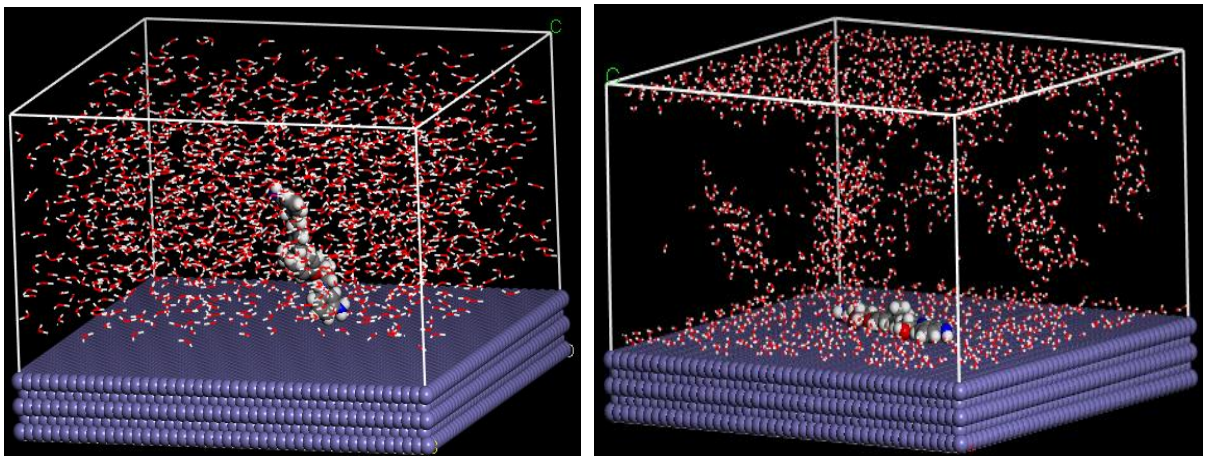

Figure 4.19: (i) Docking and (ii) adsorption of DGEBA-BDA coating molecule on mild steel surface, before and after forcite quench simulation in 3.5% wt. NaCl solution, respectively.

4.3.2 Adsorption of chitosan-reinforced epoxy (DGEBA-BDA) coating molecules on mild steel surface

The docking and adsorption behaviours of chitosan-reinforced epoxy (DGEBA-BDA) coating are presented in Figure 4.20 below.

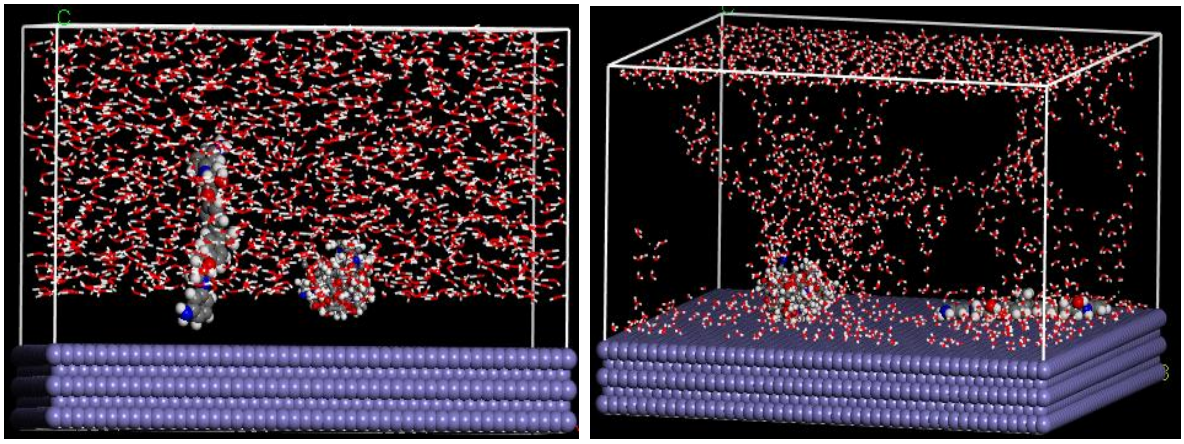

Figure 4.20: (i) Docking of chitosan-reinforced DGEBA-BDA coating molecule on mild steel surface before and (ii) adsorption of chitosan-reinforced DGEBA-BDA coating molecule on mild steel surface after forcite quench simulation in 3.5% wt. NaCl solution.

It can be observed that that the composite coating adsorbs on the mild steel surface in a flat orientation. This also shows that the composite coating can interact with the mild steel surface via its active sites present in both the epoxy

and the chitosan nanocluster and consequently has the potential to perform as a good anticorrosion coating.

4.3.3 Silane modification of chitosan nanocluster

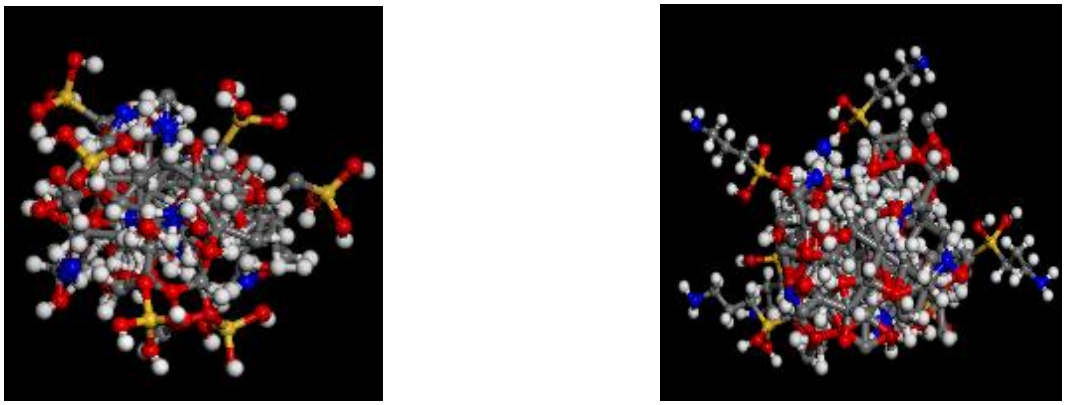

(i) (ii)

Figure 4.21: (i) tetraethoxy silane (TEOS)-modified chitosan nanocluster, (ii) (3-Aminopropyl ethoxy) silane (APES)-modified chitosan nanocluster

4.3.3 Adsorption of epoxy coating reinforced with silane-modified chitosan nanocluster on mild steel surface.

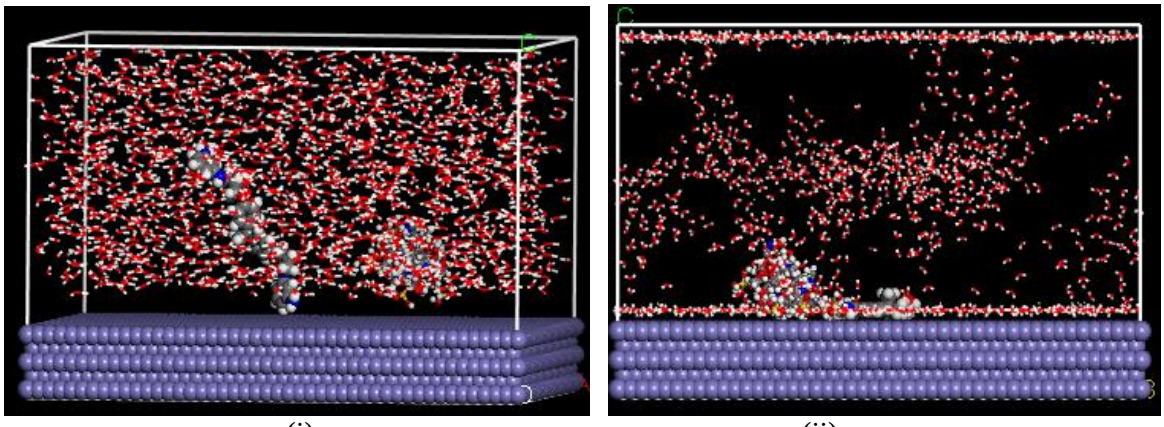

(i) (ii)

Figure 4.22: (i) Docking and (ii) adsorption of epoxy coating molecules reinforced with TEOS-modified chitosan nanocluster on mild steel surface, before and after forcite quench simulation in 3.5% wt. NaCl solution, respectively.

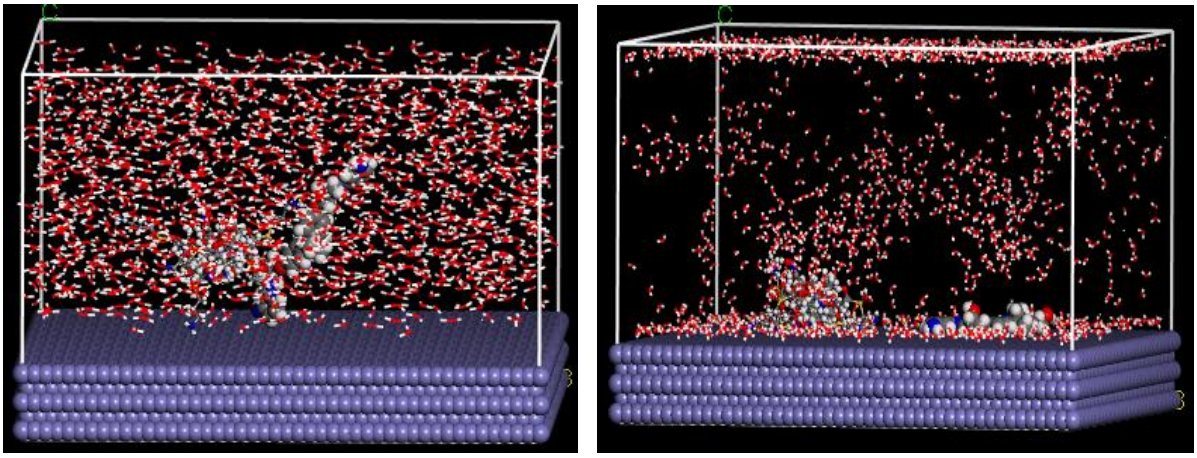

(i) (ii)

Figure 4.23: (i) Docking and (ii) adsorption of epoxy coating molecules reinforced with APTES-modified chitosan nanocluster on mild steel surface, before and after forcite quench simulation in 3.5% wt. NaCl solution, respectively.

Figure 4.22 & 4.33 shows the adsorption behaviours of TEOS-chitosan and APTES-chitosan on mild steel. We also observed that the composite adsorbs on mild steel substrate in a flat orientation. Thus, we expect the composites to perform as a good anticorrosion coating for mild steel.

4.3.4 Bond length analysis via radial distribution function

The radial distribution function which helps to determine the bond length of interacting molecules can be calculated using MD simulation. This parameter gives an insight into the type of interaction between two or more interacting molecules. The interaction between two or more molecules can be a chemical adsorption (chemisorption) or a physical adsorption (physisorption). Chemical adsorption is associated with shorter bond length between 1.0 and 3.5A, and gives high bond strength, while physical adsorption is marked by bond length greater than 3.5A and correspondingly indicates lower bond strength (Dagdag et al., 2019). Thus, if the interaction between a coating molecule and metal substrate is a chemical interaction, a high bond strength is expected and consequently the molecule is expected to perform as a good corrosion inhibitor. However, physical

interaction is usually marked by shorter bond length and consequently poor bond strength and the molecule might not perform well as a good anticorrosion coating.

Thus, the bond length of the atoms of DGEBA-BDA with respect to mild steel were analysed using the radial distribution function. Figure 4.24 shows the graphical representation of the radial distribution function.

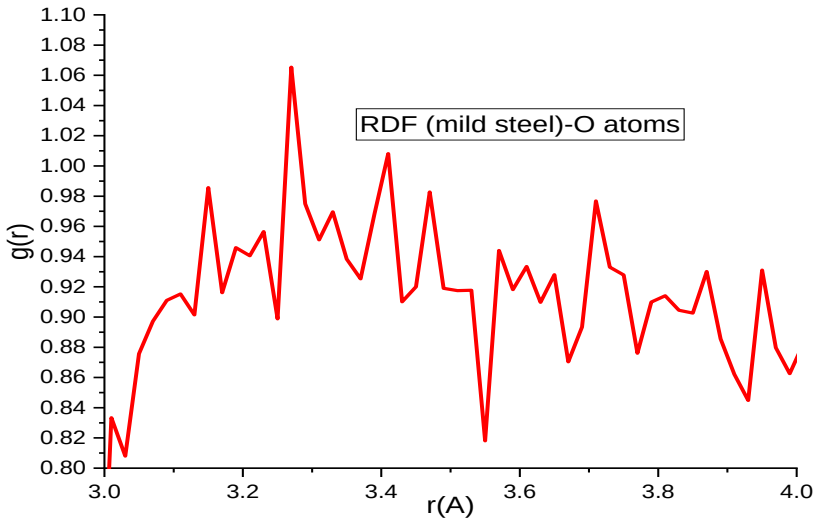

(i)

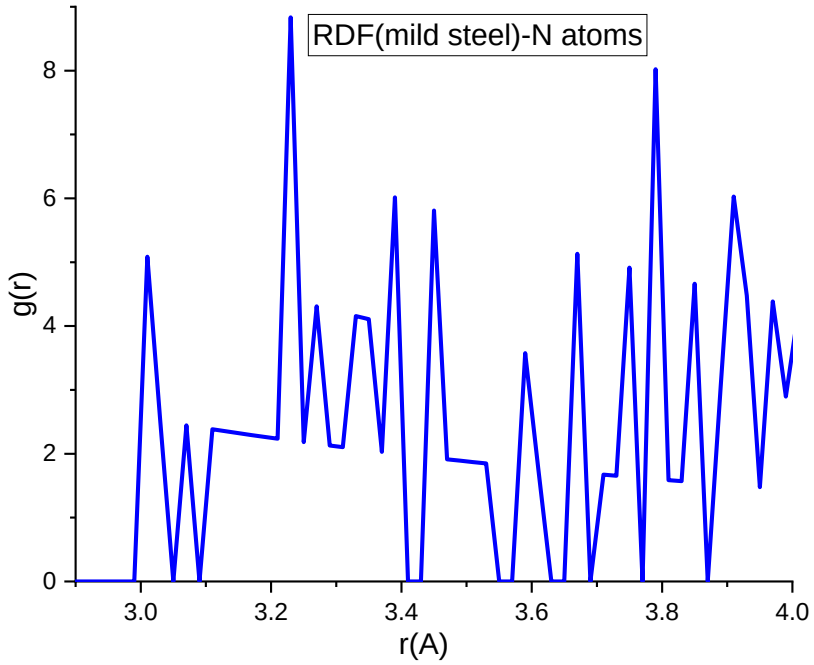
RDF(mild steel)-N atoms
g(r)
r(A)
0
2
4
6
8
3.0
3.2
3.4
3.6
3.8
4.0

(ii)

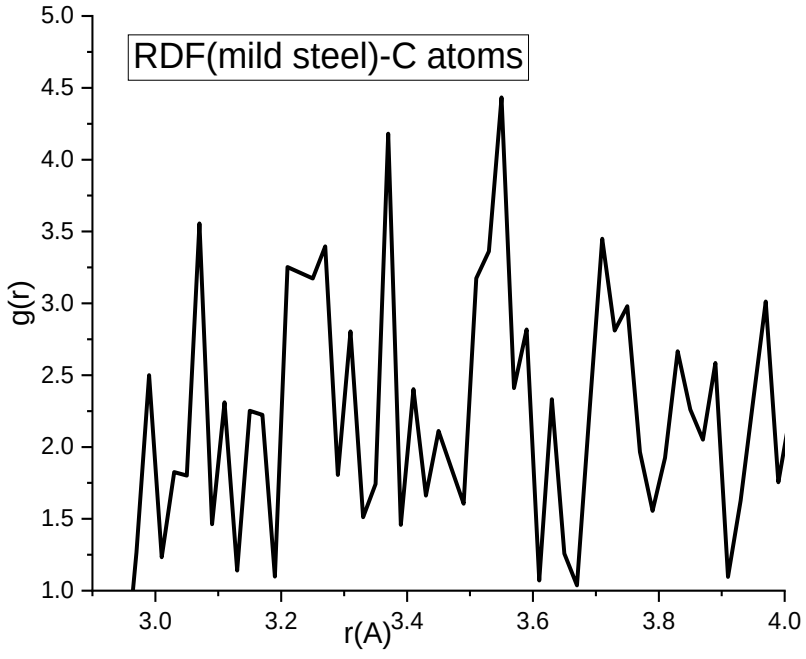
RDF(mild steel)-C atoms
g(r)
r(A)
1.0
1.5
2.0
2.5
3.0
3.5
4.0
4.5
5.0
3.0
3.2
3.4
3.6
3.8
4.0

(iii)

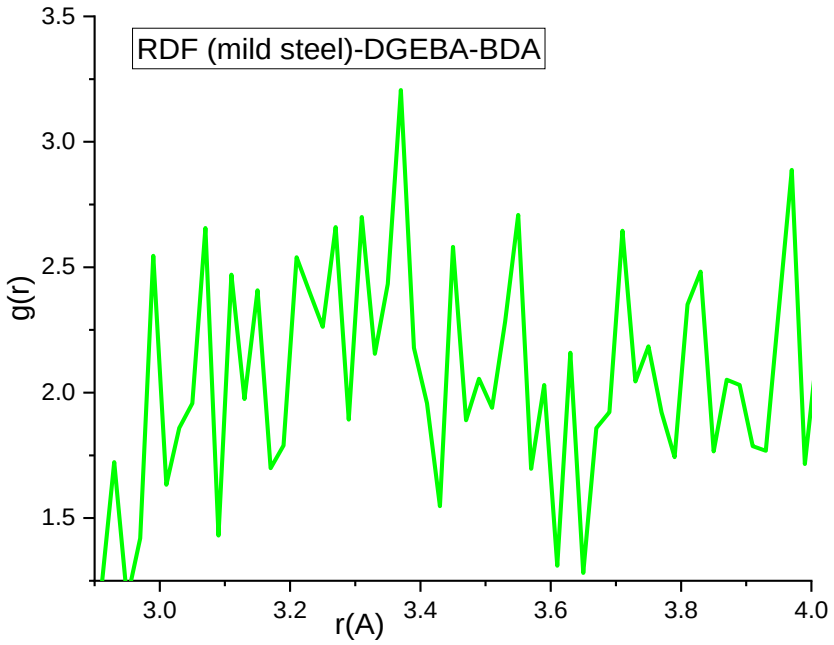

(iv)

Figure 4.24: Graphical representation of RDF for (i) mild steel – O atoms, (ii) mild steel – N atoms, (iii) mild steel – C atoms and (iv) mild steel – epoxy coating (DGEBA-BDA) monomer.

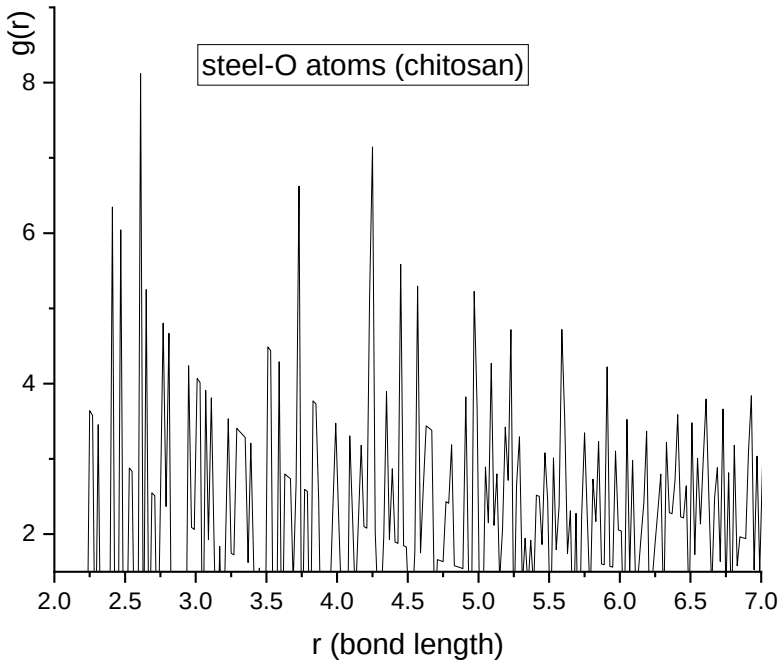
steel-O atoms (chitosan)
g(r)
8
6
4
2
2.0
2.5
3.0
3.5
4.0
4.5
5.0
5.5
6.0
6.5
7.0
r (bond length)

(i)

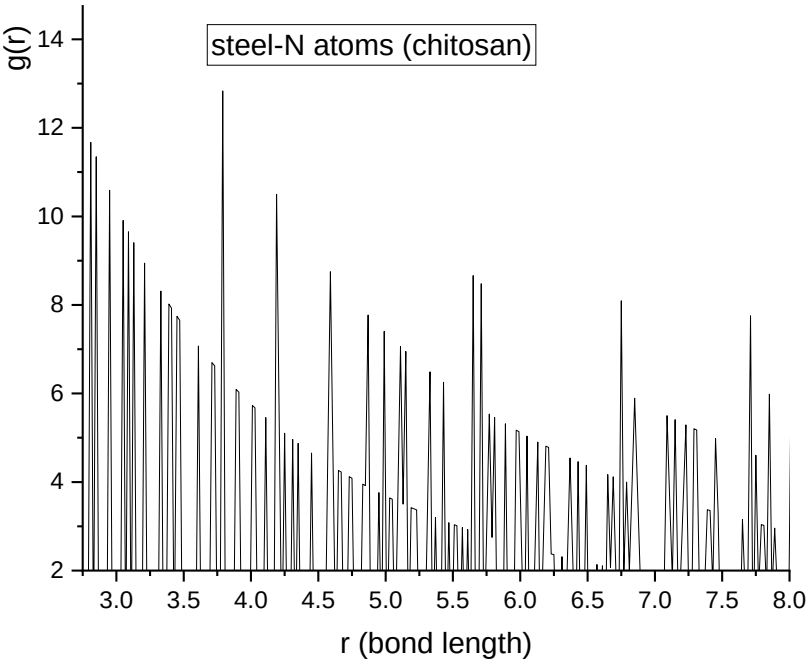
steel-N atoms (chitosan)
g(r)
14
12
10
8
6
4
2
3.0
3.5
4.0
4.5
5.0
5.5
6.0
6.5
7.0
7.5
8.0
r (bond length)

(ii)

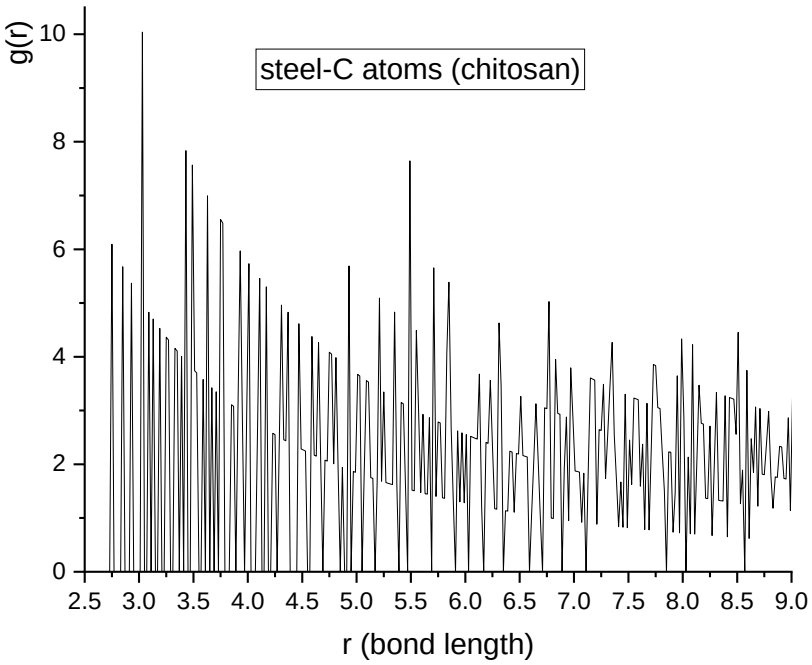

(iii)

Figure 4.25: Graphical representation of RDF for (i) mild steel – O atoms, (ii) mild steel – N atoms, (iii) mild steel – C atoms of chitosan nanocluster

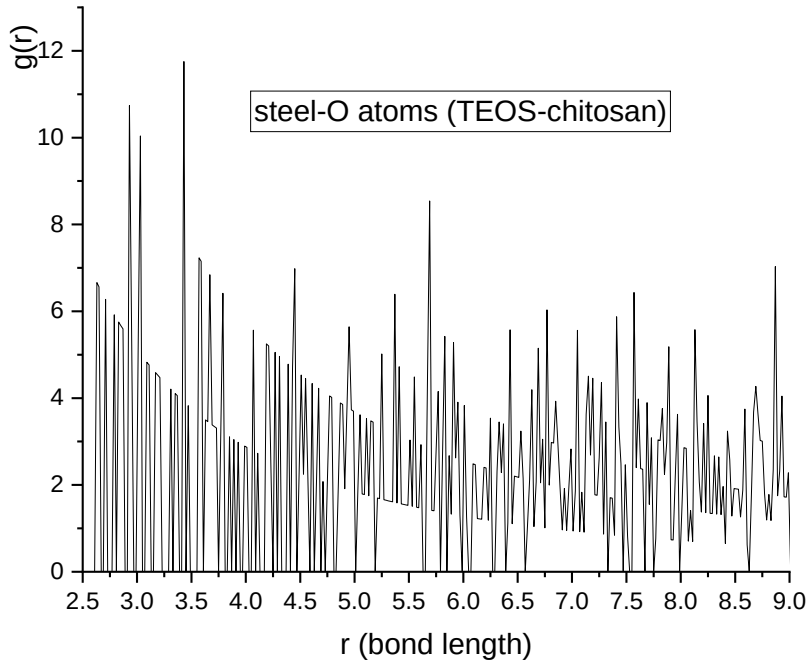
g(r)
steel-O atoms (TEOS-chitosan)
r (bond length)

(i)

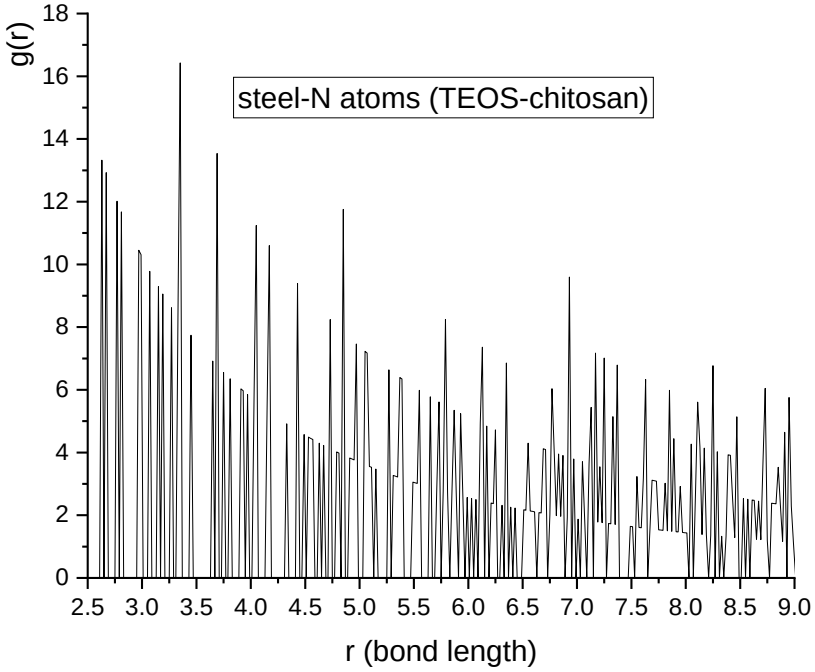
g(r)
steel-N atoms (TEOS-chitosan)
r (bond length)

(ii)

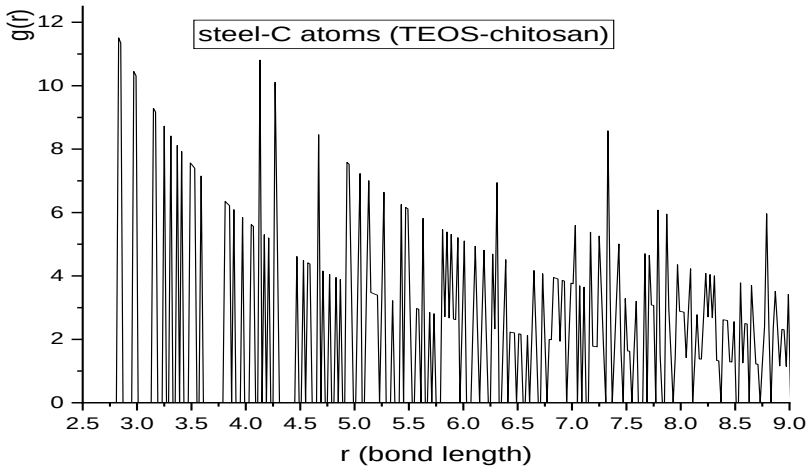

(iii)

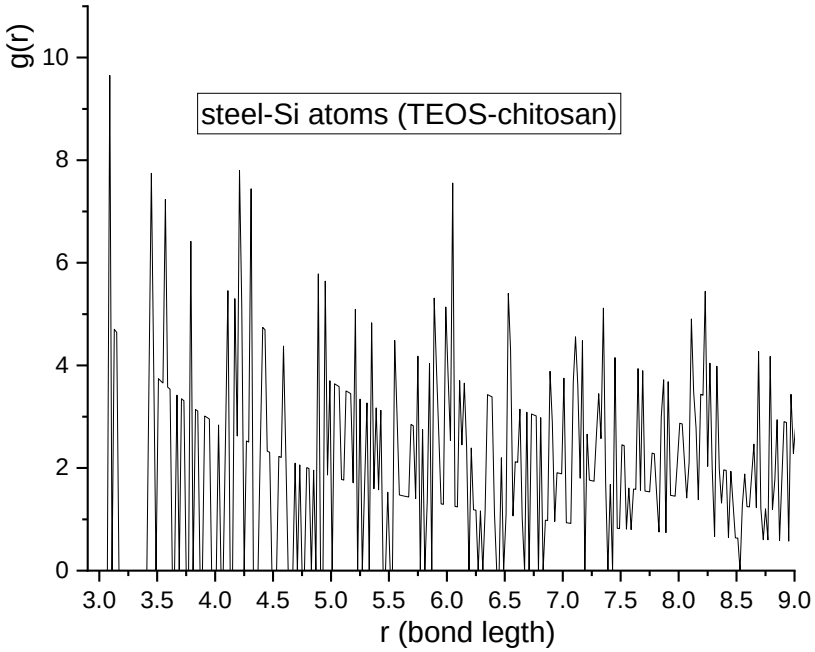

(iv)

Figure 4.26: Graphical representation of RDF for (i) mild steel – O atoms, (ii) mild steel – N atoms, (iii) mild steel – C atoms and (iv) mild steel-Si atoms of TEOS- chitosan nanocluster

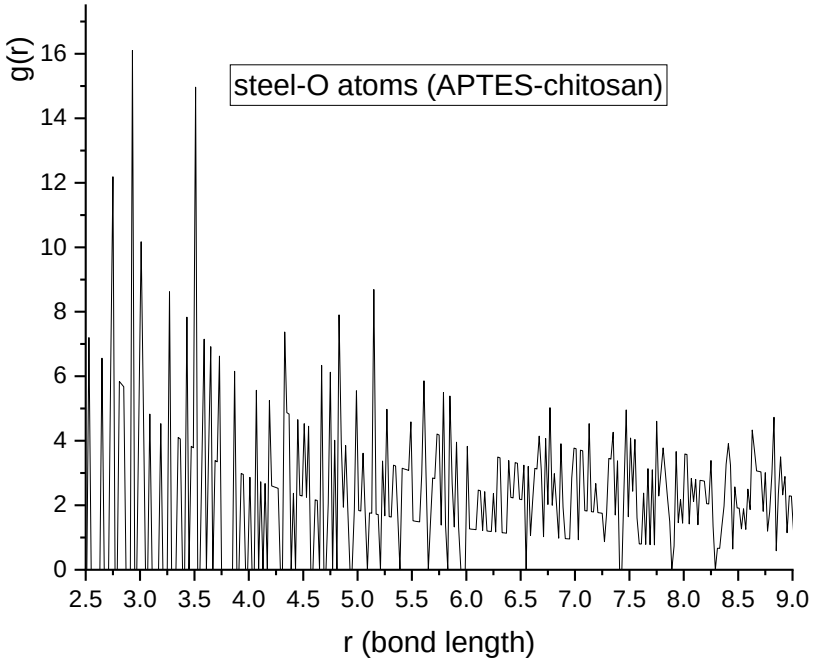
g(r)
steel-O atoms (APTES-chitosan)
0
2
4
6
8
10
12
14
16
2.5 3.0 3.5 4.0 4.5 5.0 5.5 6.0 6.5 7.0 7.5 8.0 8.5 9.0
r (bond length)

(i)

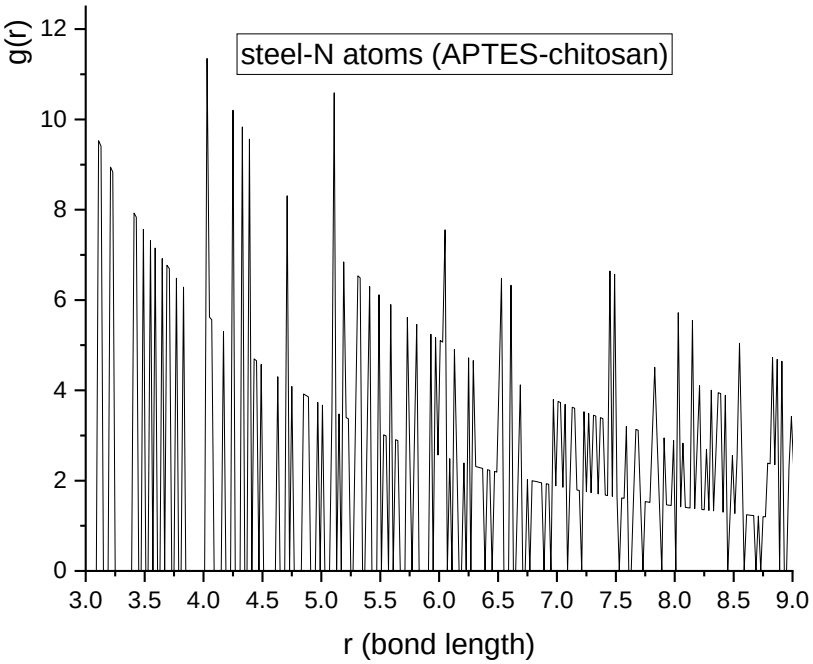
g(r)
steel-N atoms (APTES-chitosan)
0
2
4
6
8
10
12
3.0 3.5 4.0 4.5 5.0 5.5 6.0 6.5 7.0 7.5 8.0 8.5 9.0
r (bond length)

(ii)

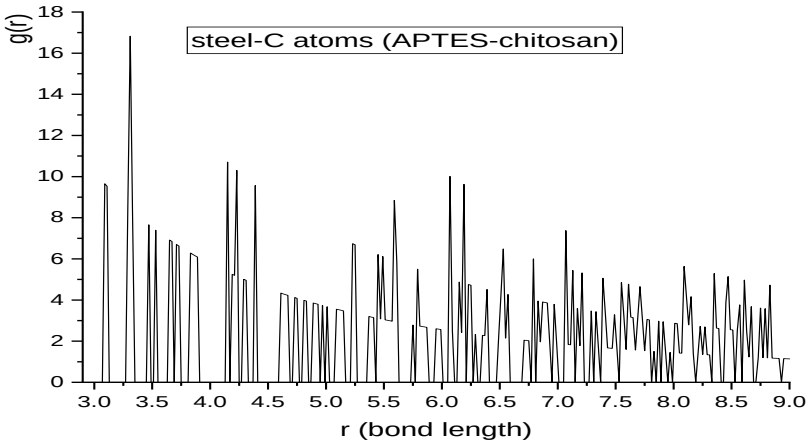

(iii)

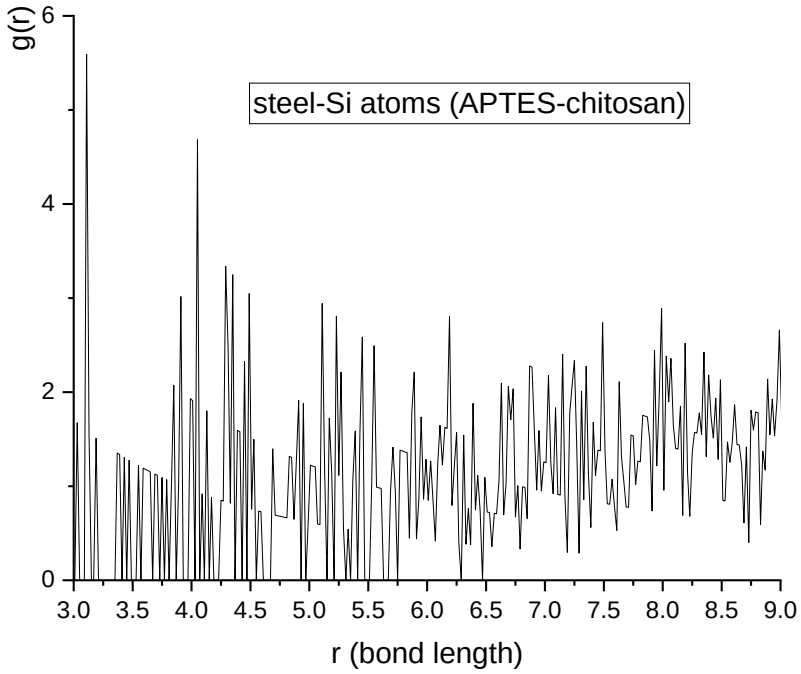

Figure 4.27: Graphical representation of RDF for (i) mild steel – O atoms, (ii) mild steel – N atoms, (iii) mild steel – C atoms and (iv) mild steel-Si atoms of APTES- chitosan nanocluster

The extracted results given in Table 4.9 show that the interaction between the oxygen atom, nitrogen atoms and carbon atoms in DGEBA-BDA with respect the mild steel is associated with bond lengths of 3.27A, 3.25A and 3.55A respectively. It is clear that the interaction between DGEBA-BDA and mild steel is both chemical and physical adsorption. In other to ascertain the predominant type of adsorption, the RDF between the DGEBA-BDA monomer and mild steel was analysed and result showed that the bond length is 3.37A which is less than 3.5A. Thus, we can conclude that the interaction between DGEBA-BDA and mild steel is mainly a chemisorption, this means that the DGEBA-BDA can adhere to mild steel substrate and can perform as a good anticorrosion coating. Table 4.9 summarizes the bond length of DGEBA-BDA/mild steel interaction

Table 4.9: Bond length of atoms of epoxy (DGEBA-BDA) monomer with respect to mild steel surface.

steel–coating atoms interaction	Steel - O	Steel - N	Steel - C	Steel – epoxy coating
Bond length (A)	3.27	3.25	3.55	3.37

Furthermore, figures 4.25, 4.26 and 4.27 shows the RDF plots atoms of chitosan, TEOS-chitosan and APTES-chitosan respectively and Tables 4.10, 4.11 and 4.12 summarizes the bond length of individual atoms of chitosan, TEOS-chitosan and APTES-chitosan respectively with respect to mild steel surface. It is clear that the interaction of O, C & Si present in chitosan nanocluster as well the silane modified chitosan nanocluster with respect to mild steel is associated with bond length less than 3.5A. thus, we can conclude that these atoms enhance chemical adsorption of both chitosan and silane modified chitosan unto mild steel substrate

Table 4.10: Bond length of atoms of chitosan nanocluster with respect to mild steel surface.

interaction	bond length (A)
Steel-O atoms	2.61
Steel-N atoms	3.79
Steel-C atoms	3.03

Table 4.11: Bond length of atoms of TEOS-chitosan nanocluster with respect to mild steel surface.

interaction	RDF bond length (A)
Steel-O atoms	3.43
Steel-N atoms	3.35
Steel-C atoms	2.85
Steel-Si atoms	3.09

Table 4.12 Bond length of atoms of APTES-chitosan nanocluster with respect to mild steel surface.

interaction	bond length (A)
Steel-O atoms	2.93
Steel-N atoms	4.03
Steel-C atoms	3.31
Steel-Si atoms	3.11

4.3.5 Adsorption energies of different formulations of epoxy coating on mild steel surface

The adsorption energy is another important parameter that is used to determine the adsorption strength of (DGEBA-BDA)-mild steel interaction. This parameter gives an insight into the bonding strength of the coating molecule with

mild steel and this can be used to predict the anticorrosion performance of the coating molecule. Studies have shown that molecules with higher negative value of adsorption energy on mild steel is expected to form stronger bonds with the mild steel surface and consequently provides a better anticorrosion performance for the mild steel substrate (Dagdag et al., 2019; Uwakwe et al., 2016).

Herein, the MD simulation was used to determine the adsorption energy between coating molecule and mild steel substrate. The DGEBA-BDA was further reinforced with chitosan nanocluster and chitosan nanocluster modified with different silane coupling agents and the adsorption energies were determined accordingly using the established equation(Dagdag et al., 2020):

$$E_{ads} = E_{total} - \left(E_{surface+solution} + E_{coating+solution}\right) + E_{solution} \qquad (4.1)$$

Where;

E_{ads} = adsorption energy,

E_{total} = single point energy of the whole system,

$E_{surface+solution}$ = single point energy for mild steel + 3.5 wt% NaCl solution, $E_{coating+solution}$ = single point energy for DGEBA-BDA + 3.5wt% NaCl solution, and $E_{solution}$ = single point energy for 3.5wt% NaCl solution

The results for the single point energy calculations are given below for the different coating compositions.

Table 4.13: Energy calculation for adsorption of epoxy monomer on mild steel surface in 3.5 wt.% salt solution.

Component	Value	kcal/mol
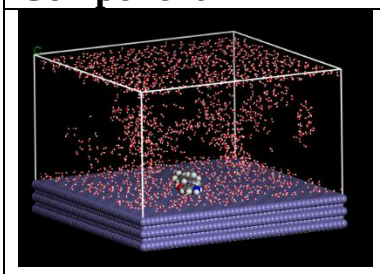	E_{total}	-31881.035761
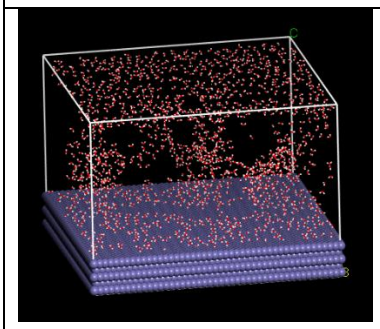	$E_{surface+solution}$	-30692.305776
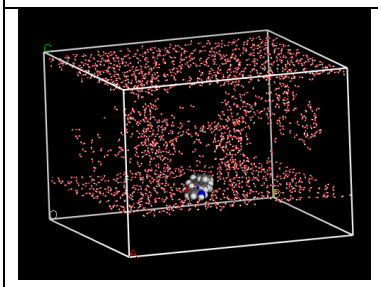	$E_{coating+solution}$	-13928.805829
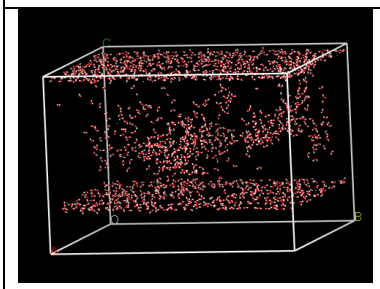	$E_{solution}$	-13929.410909

$$\mathbf{E_{adsorption} = E_{total} - (E_{surface/solution} + E_{coating/solution}) + E_{solution} = -1{,}189.64\ kcal/mol}$$

Table 4.14: Energy calculation for adsorption of chitosan-reinforced epoxy coating on mild steel in 3.5wt% NaCl solution

Component	Value	kcal/mol
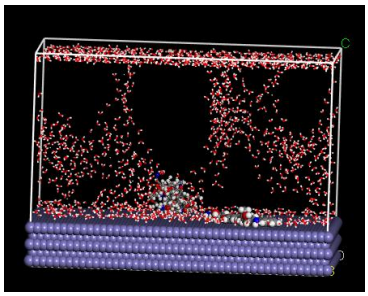	E_{total}	44074.042672
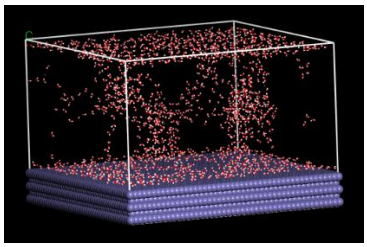	$E_{surface+solution}$	-28932.653107
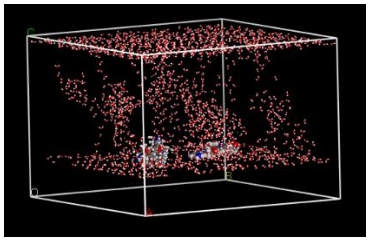	$E_{coating+solution}$	61348.179192
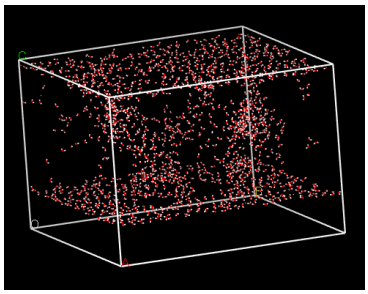	$E_{solution}$	-13964.279571

$E_{ads} = E_{total} - (E_{surf+sol} + E_{coating+sol}) + E_{sol}$ = -2,306.42 kcal/mol

Table 4.15: Energy calculation for adsorption of epoxy coating reinforced with TEOS-modified chitosan nanocluster on mild steel surface in 3.5 wt.% NaCl solution.

Component	**Value**	**kcal/mol**
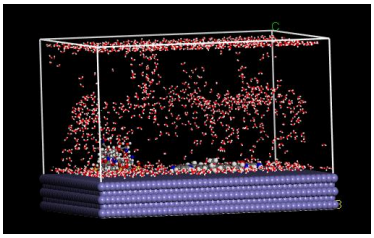	E_{total}	44041.213025
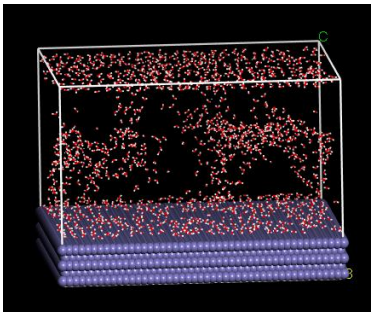	$E_{surface+solution}$	-28321.314099
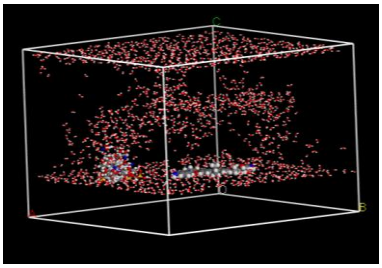	$E_{coating+solution}$	62151.960119
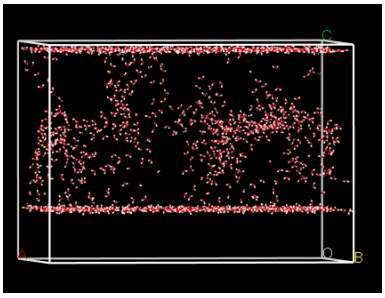	$E_{solution}$	-12841.048401

$E_{ads} = E_{total} - (E_{surface/solution} + E_{coat/solution}) + E_{sol}$ = -2,630.00 kcal/mol

Table 4.16: Energy calculation for adsorption of epoxy coating reinforced with APTES-modified chitosan nanocluster on mild steel surface in 3.5 wt.% NaCl solution.

Component	**Value**	**kcal/mol**
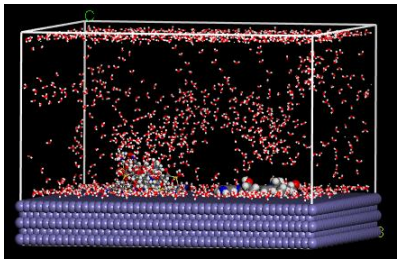	E_{total}	43744.403263
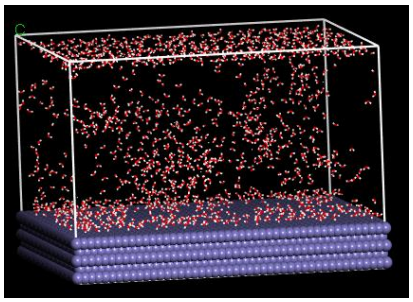	$E_{surface+solution}$	-28323.823533
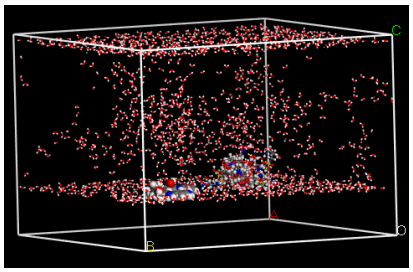	$E_{coating+solution}$	62532.113695
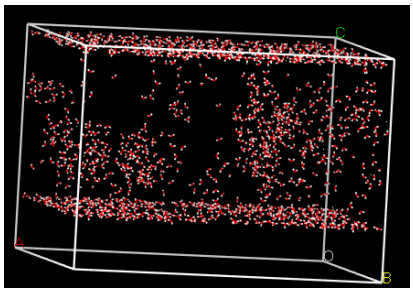	$E_{solution}$	-12630.763012

$E_{ads}=E_{total} - (E_{surf/sol} + E_{coat/sol}) + E_{sol.}$ = - 3,094.65 kcal/mol

Table 4.17: Summary of adsorption energies and protection potential index of different formulations of coatings on mild steel surface.

ID	Coating formulation	Adsorption energy (kcal/mol)	$\%P_c$	$\%P_{ch}$
(i)	Epoxy monomer	- 1,189.33	-	-
(ii)	Chitosan reinforced epoxy coating	- 2,305.77	48.42	-
(iii)	TEOS-modified chitosan /epoxy monomer	- 2,630.00	54.78	12.33
(iv)	APTES-modified chitosan/epoxy monomer	- 3,094.65	61.58	25.49

Table 4.17 summarizes the adsorption energy results for different DGEBA-BDA formulation. Results showed that DGEBA-BDA is associated with high negative value of energy of adsorption which is higher than previously reported epoxy monomer (Dagdag et al., 2019; Dagdag et al., 2020). Coating molecules with high negative value of adsorption energy is usually associated with good barrier or anticorrosion performance. The negative value indicates a spontaneous interaction with mild steel. Again, it was observed that addition of chitosan nanocluster consequently increased the negativity of the adsorption energy of the coating. This result shows that addition of chitosan nanocluster can improve the anticorrosion performance of DGEBA-BDA. Furthermore, the addition of silane modified chitosan nanocluster further increased the negativity of the adsorption energy of DGEBA-BDA in the order; APTEO > TEOS. In addition, the protection potential performance index of the composite coating over epoxy monomer was calculated (see Table4.17) and result showed that APTES-chitosan modified epoxy coating has the potential (61.58%) to perform as a better anticorrosion coating compared to others. On the other hand, the protection potential performance over unsilanized epoxy coating was obtained and results also showed that silane modified epoxy/chitosan composite coating

has a potential to perform as a good anticorrosion coating with APTES modified chitosan having the best potential. These results are in agreement with the findings of (Arukalam et al., 2021). Thus, we can conclude that addition of silane modified chitosan into DGEBA-BDA based coating system can improve the anticorrosion performance of DGEBA-BDA.

4.3 Anti-Fouling Potential Evaluation via Molecular Dynamic (MD) Simulation

MD simulation was employed to understand the adsorption behaviour of mussel protein (L-DOPA) on mild steel substrate which serve as the blank and also how it adsorbs on epoxy coating, chitosan modified epoxy composite coating and silane modified chitosan/epoxy composite coating. This adsorption behaviour of L-DOPA on these substrates gives an insight into the antifouling potential of the different substrate studied. Figure 4.28 shows the adsorption of L-DOPA on bare mild steel in the presence of simulated salt water. It can be seen that mussel protein (L-DOPA) acquires a flat orientation on the surface of the bare mild steel in simulated seawater with a high adsorption energy (see table 4.22). This implies that the protein can adsorb on steel surface which can lead to the colonization of steel surface by marine organisms.

Furthermore, the adsorption of L-DOPA on epoxy surface was investigated using MD simulation, results showed that the interaction was minimal with a lower adsorption energy (see figure 4.29 & Table 4.22). however, when the epoxy surface was reinforced with chitosan nanocluster, the interaction was further minimized with a low adsorption energy. In addition, we observed a very minimal interaction between L-DOPA and epoxy/TEOS-chitosan nanocluster surface. Again, incorporation of APTES-chitosan nanocluster into the epoxy surface further reduced the adsorption energy of L-DOPA on the coating surface (see figures4.29 & 4.30). Table 4.22 summarizes the adsorption energy of L-DOPA on the different substrates. It can be observed that epoxy coating modified with

silane additives are associated with low adsorption energy with APTES-chitosan having the lowest adsorption energy. (Gao, 2021) has shown that lower adsorption energy of mussel-polymer surface interaction is associated with antifouling capability of the surface. Hence, this implies that APTES-chitosan modified epoxy has the potential to perform as a better foul resistance surface to L-DOPA compared to other surfaces studied in this work.

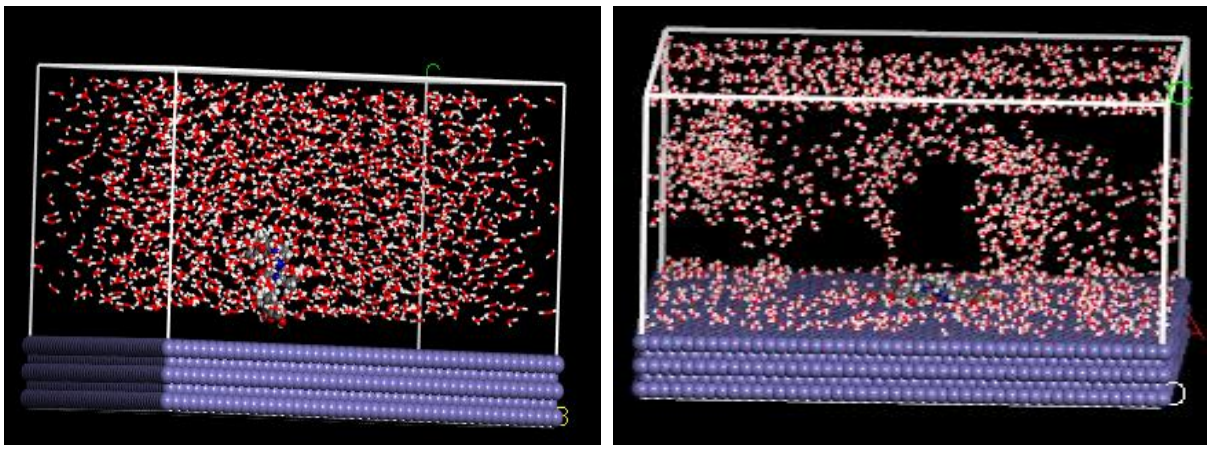

(i) (ii)

Figure 4.28: (i) Docking and (ii) adsorption of L DOPA on bare mild steel surface, before and after forcite quench simulation in 3.5% wt. NaCl solution, respectively.

Table 4.18: Energy calculation for adsorption of L-DOPA on mild steel surface in 3.5 wt.% NaCl solution.

Component	Value	kcal/mol
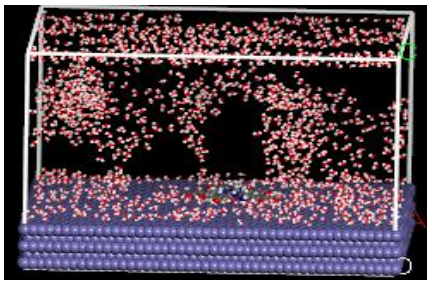	E_{total}	-30950.298158
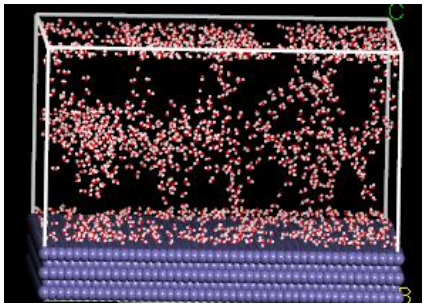	$E_{surface+solution}$	-29,141.84434
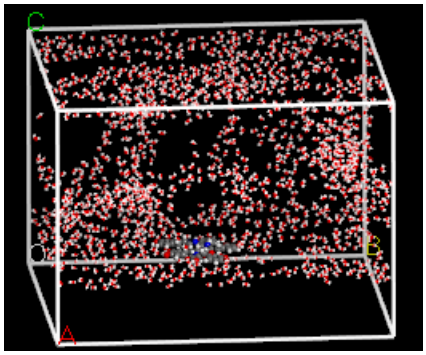	$E_{protein+solution}$	-14327.141797
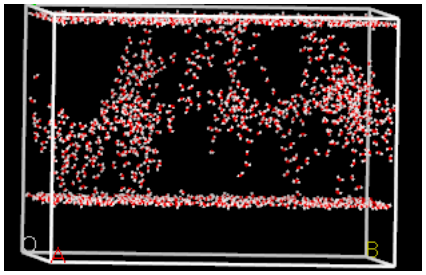	$E_{solution}$	-14340.270881

$$E_{ads} = E_{total} - (E_{surf\_solution} + E_{protein\text{-}solution}) - E_{solution} = -1{,}831.58 \text{ kcal/mol}$$

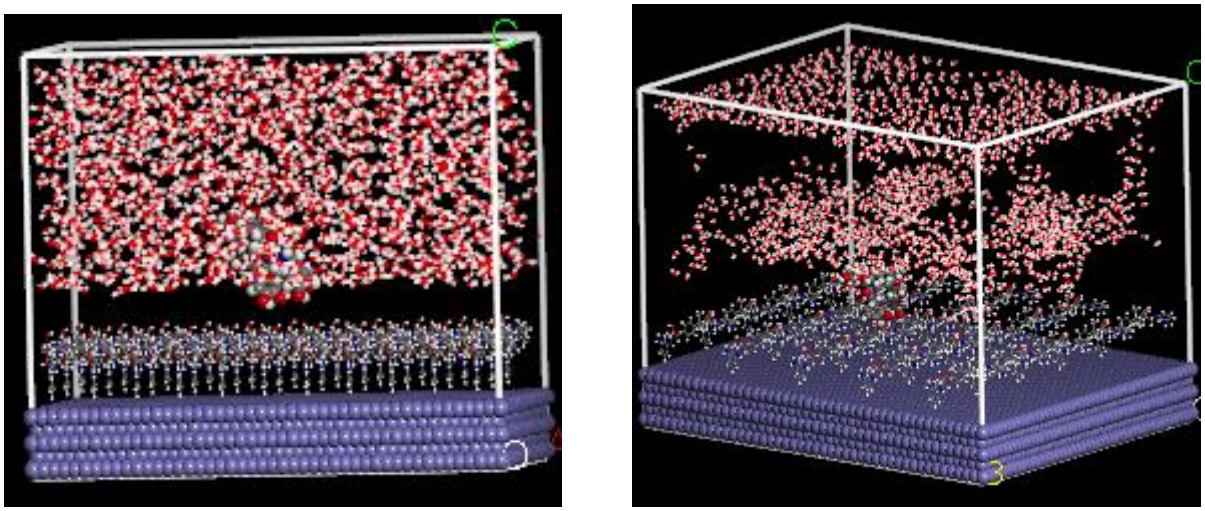

(i) (ii)

Figure 4.29: (i) Docking and (ii) adsorption of L DOPA on epoxy-coated mild steel surface, before and after forcite quench simulation in 3.5% wt. NaCl solution, respectively.

Table 4.19: Energy calculation for adsorption of L-DOPA on epoxy surface in 3.5 wt.% NaCl solution.

Component	Value	kcal/mol
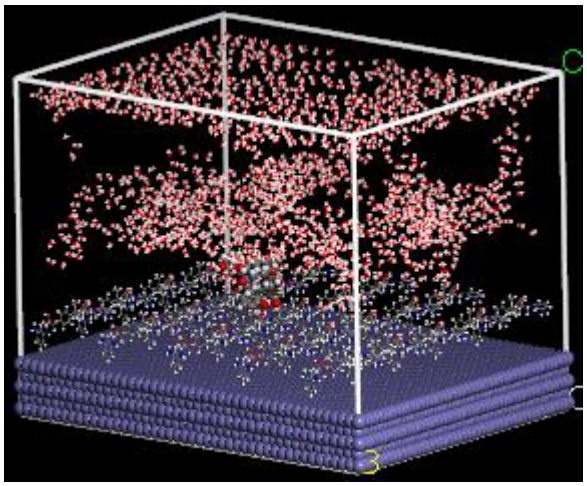	E_{total}	-22308.129224
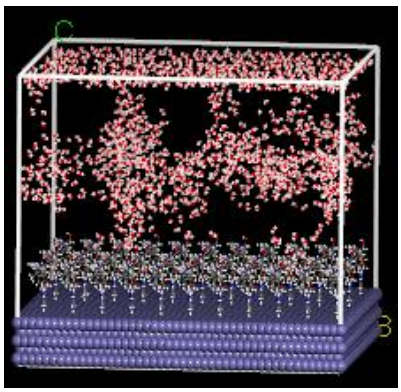	$E_{surface+solution}$	-21842.859202
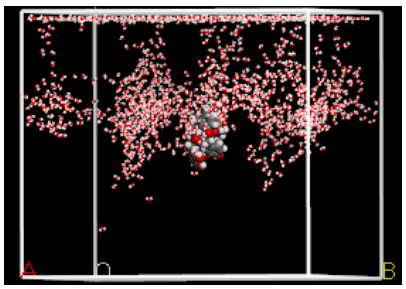	$E_{protein+solution}$	-14911.442969
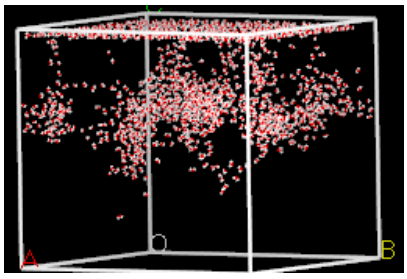	$E_{solution}$	-14750.448636

$$E_{ads} = E_{total} - (E_{surf\_solution} + E_{protein\text{-}solution}) + E_{solution} = -304.27 kcal/mol$$

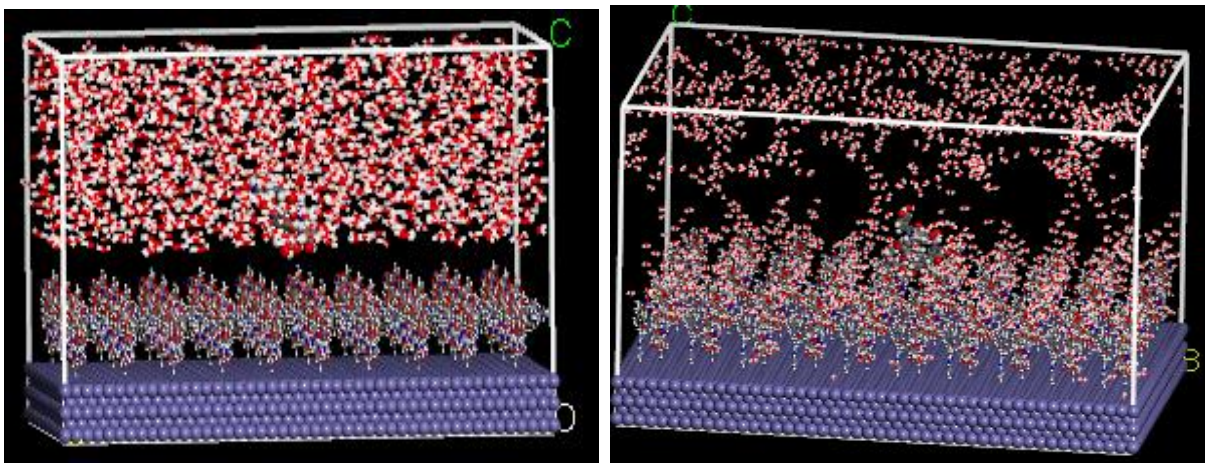

(i) (ii)

Figure 4.30: (i) Docking and (ii) adsorption of L DOPA on chitosan-modified epoxy coated mild steel surface, before and after forcite quench simulation in 3.5% wt. NaCl solution, respectively.

Table 4.20: Energy calculation for adsorption of L-DOPA on epoxy/chitosan surface in 3.5 wt.% NaCl solution.

Component	Value	kcal/mol
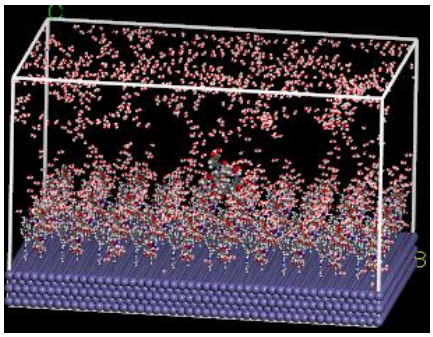	E_{total}	-31929.989174
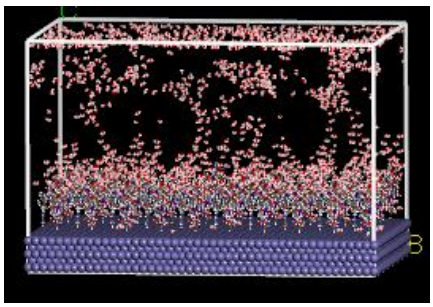	$E_{surface+solution}$	-31723.845401
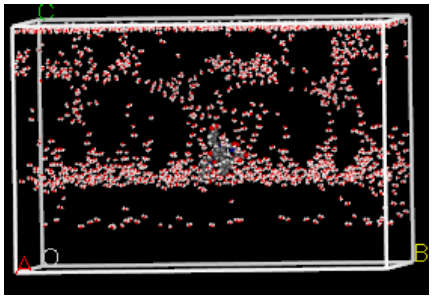	$E_{protein+solution}$	-6172.285294
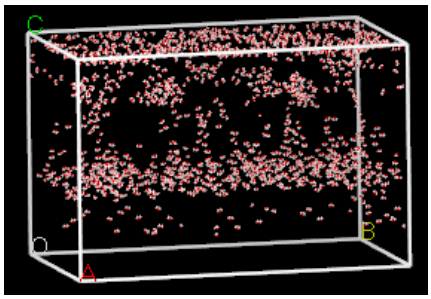	$E_{solution}$	-6155.445143

$E_{ads} = E_{total} - (E_{surf\_solution} + E_{protein-solution}) - E_{solution}$ = -189.3 kcal/mol

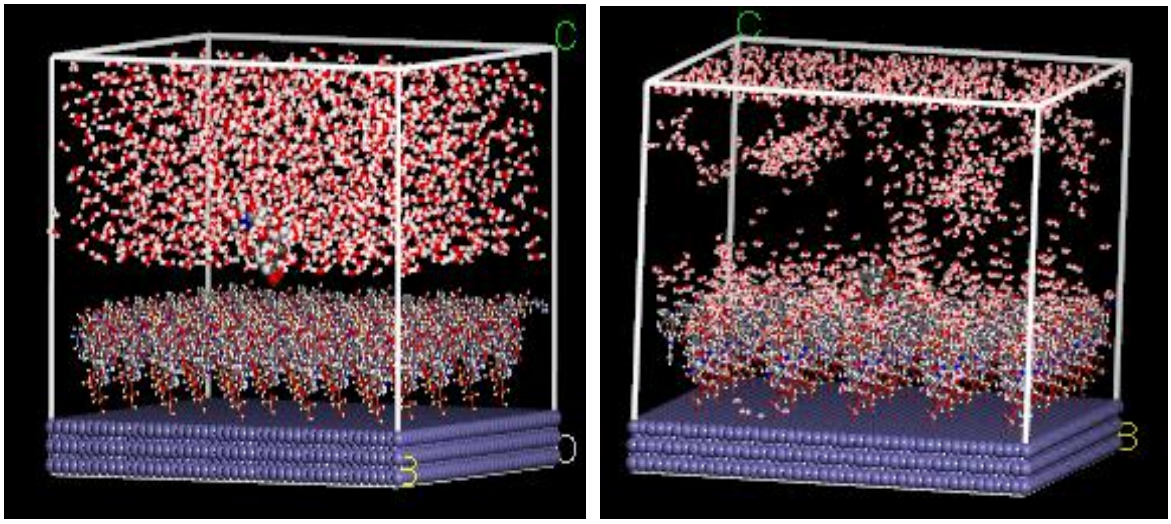

(i) (ii)

Figure 4.31: (i) Docking and (ii) adsorption of L DOPA on epoxy coating reinforced with TEOS-modified chitosan nanocluster, before and after forcite quench simulation in 3.5% wt. NaCl solution, respectively.

Table 4.21: Energy calculation for adsorption of L-DOPA on epoxy coating reinforced with TEOS-modified chitosan nanocluster in 3.5 wt.% NaCl solution.

Component	Value	kcal/mol
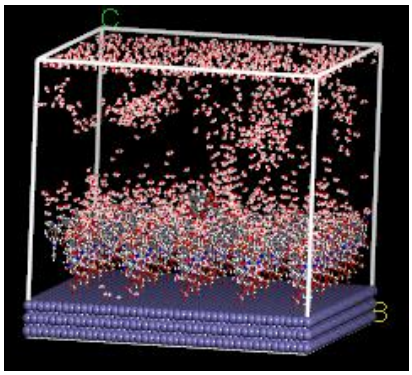	E_{total}	-29614.367338
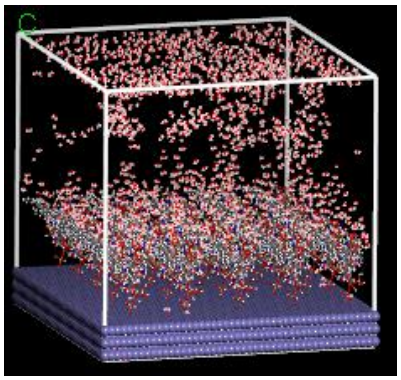	$E_{surface+solution}$	-29404.966932
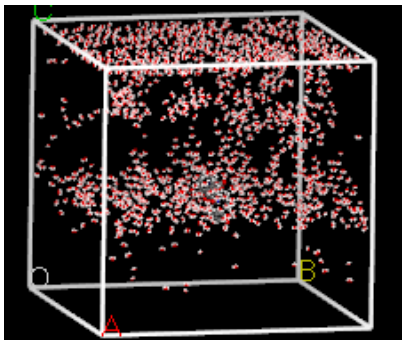	$E_{protein+solution}$	-8455.446914
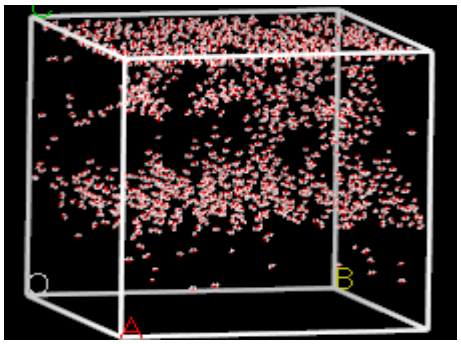	$E_{solution}$	-8388.482987

$$E_{ads} = E_{total} - (E_{surf\_solution} + E_{protein\text{-}solution}) + E_{solution} = -142.44 kcal/mol$$

4.4.5 Interaction of mussel peptide with epoxy/ amino silane modified chitosan protected mild steel

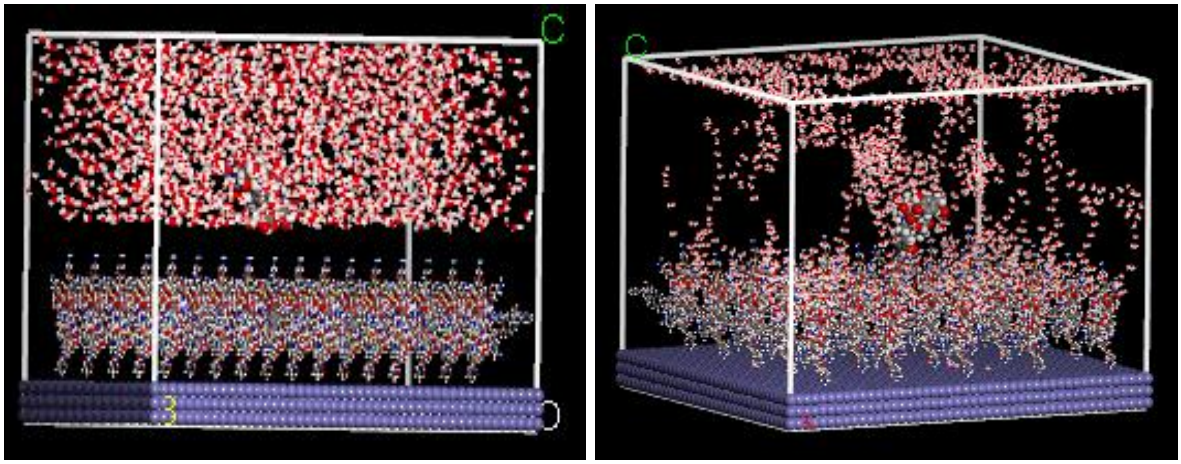

(i) (ii)

Figure 4.32: (i) Docking and (ii) adsorption of L DOPA on epoxy coating reinforced with APTES-modified chitosan nanocluster, before and after forcite quench simulation in 3.5% wt. NaCl solution, respectively.

Table 4.22: Energy calculation for adsorption of L-DOPA on epoxy coating reinforced with APTES-modified chitosan in 3.5 wt.% NaCl solution.

Component	Value	kcal/mol
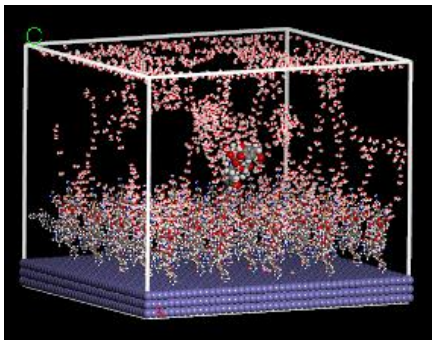	E_{total}	-29240.077068
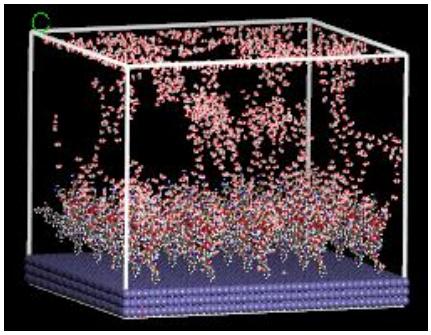	$E_{surface+solution}$	-29048.764186
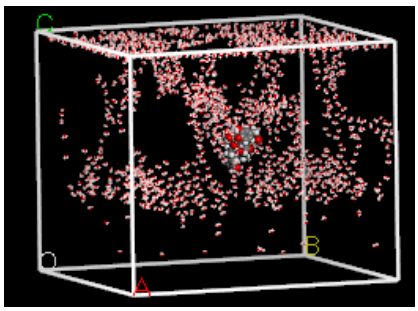	$E_{protein+solution}$	-9976.689927
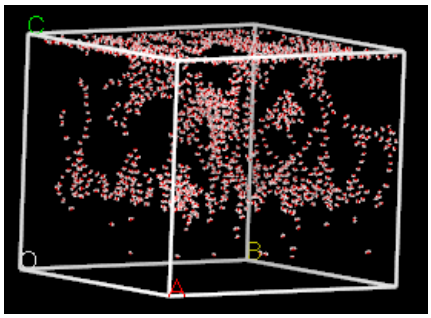	$E_{solution}$	-9837.811702

$$E_{ads} = E_{total} - (E_{surf\_solution} + E_{protein\text{-}solution}) + E_{solution} = -52.44 \text{ kcal/mol}$$

Table 4.23: Summary of adsorption energies of mussel peptide (L DOPA) on bare steel surface and steel surface protected with different formulations of epoxy coating on mild steel surface.

substrate	Adsorption energy (kcal/mol)	(%A_P)	(%A_{pE})
Bare steel surface	-1831.58	-	-
Epoxy coating	-304.27	83.38	-
Chitosan reinforced epoxy coating	-189.30	89.66	37.78
Epoxy coating reinforced with TEOS-modified chitosan nanocluster	-142.44	92.22	53.18
Epoxy coating reinforced with APES-modified chitosan nanocluster	-52.44	97.13	82.76

From Table 4.23 above, it can be seen that when the bare steel was covered with epoxy coating, the increase in antifouling potential efficiency over the uncoated metal was observed to be 83.38%. when the coating was modified with chitosan, the antifouling potential efficiency over bare metal surface increased to 89.66%, furthermore, when the coating was modified with TEOS and APTES, the antifouling potential efficiency over the bare metal further increased to 92.22% and 61.58% respectively. However, the antifouling potential efficiency (%A_{pE}) of the chitosan/epoxy and silane modified chitosan/eepoxy over the unmodified epoxy coating was estimated. The antifouling potential efficiency of 37.78%, 53.18% and 82.76% were estimated for chitosan/epoxy, TEOS-chitosan/epoxy and APTES-chitosan/epoxy coating respectively. This shows that silane modified chitosan dispersed in epoxy coating matrix has the potential to perform as a good antifouling coating for mild steel.

CHAPTER FIVE

CONCLUSION AND RECOMMENDATION

5.1 Conclusion

The effect of silane modification of chitosan on anticorrosion performance of epoxy coating has been investigated using quantum chemical computations and molecular dynamics simulation techniques. Quantum chemical computations indicate that silane-modified chitosan possessed lower energy gaps, electronegativity (χ), electron affinity (*A*) and hardness (η) with higher softness (Ϭ) and higher chemical potential (μ) than the unmodified chitosan. These observed parameters are indicators of high corrosion protective capability, and therefore suggest that silane-modified chitosan possessed higher tendency for corrosion inhibition performance than the unmodified chitosan. This could be attributed to presence of hydrophobic moieties which possess water-resistant characteristics. The MD simulation results showed that adsorption energies (E_{ads}) of the silane-modified chitosan/epoxy coating were higher (more negative) than the unsilanized chitosan/epoxy and plain epoxy coatings (less negative), and consequently suggests better anticorrosion performance. The observed effect is most pronounced with (3- aminopropyl) trimethoxy silane (APES)-modified chitosan, possibly due to presence of – OH, – N, – Si atoms of the silane additive. The Fukui functions, radial distribution function (RDF) and molecular surface area values confirmed that APES-modified chitosan possess the highest potential for corrosion protection. Based on the obtained adsorption energies and potential protection efficiencies, it could be inferred that silane-modified chitosan/epoxy coating is potentially more corrosion-resistant than the unsilanized chitosan/epoxy and plain epoxy coatings, and therefore holds promise for durable service in seawater environment.

Furthermore, incorporation of silane additives also reduced the adsorption energy of L-DOPA. This also implies that incorporating silane additive unto

DGEBA-BDA based epoxy coating can impart antifouling property unto the coating system.

Due to insufficient time to undertake the experiment on this concept, it is recommended that further studies especially experiments should be carried out to validate the findings in this study.

5.2 Contribution to knowledge

To the best of our knowledge, the study of anticorrosion performance of silane-modified chitosan filled epoxy primer coatings using quantum chemical computations (QCC) and molecular dynamics simulation (MDS) techniques has not been reported in literature before now. This study has therefore established that (3- aminopropyl) trimethoxy silane-modified chitosan nanocluster (AMCN)/epoxy coating molecules possess good anticorrosion properties, and therefore would perform well if deployed for service in saline environments.

In addition, theoretical studies on fouling and anti-fouling performances of marine coatings using so many proteins abound in literature. However, to the best of our knowledge, L-DOPA, a major component of mussel adhesive protein which aids the adhesion of marine mussel on submerged substrates has not been studied and reported in literature as a representative foulant. Interestingly, our study using molecular dynamic (MD) simulation has revealed that energy of interaction between L-DOPA and (3- aminopropyl) trimethoxy silane-functionalized chitosan-modified epoxy coating is very low. This indicates that the silane-functionalized chitosan-modified epoxy coating possess high potential to resist fouling in seawater environment.

These results are veritable contributions to the body of scientific knowledge.

REFERENCES

Afia, L., Salghi, R., Bazzi, E., Bazzi, L., Errami, M., Jbara, O., Al-Deyab, S. S., & Hammouti, B. (2011). Testing natural compounds: Argania spinosa Kernels extract and cosmetic oil as ecofriendly inhibitors for steel corrosion in 1 M HCl. *International Journal of Electrochemical Science*, *6*(11), 5918–5939.

Archana, S., & Sundaramoorthy, B. (2019). Review on biofouling prevention using nanotechnology. *Journal of Entomology and Zoology Studies*, *7*(4), 640–648.

Arukalam, I. O., Madu, I. O., & Ishidi, E. Y. (2021). High performance characteristics of Lupinus arboreus gum extract as self-healing and corrosion inhibition agent in epoxy-based coating. *Progress in Organic Coatings*, *151*, 106095. https://doi.org/10.1016/j.porgcoat.2020.106095

Arukalam, I. O., Timothy, U. J., Madu, I. O., & Achor, J. O. (2021a). Improving the Water Barrier and Anticorrosion Performances of Epoxy-Chitosan Coatings via Silane Modification. *Journal of Bio- and Tribo-Corrosion*, *7*(3). https://doi.org/10.1007/s40735-021-00512-9

Arukalam, I. O., Timothy, U. J., Madu, I. O., & Achor, J. O. (2021b). Improving the Water Barrier and Anticorrosion Performances of Epoxy - Chitosan Coatings via Silane Modification. *Journal of*

Bio- and Tribo-Corrosion. https://doi.org/10.1007/s40735-021-00512-9

Černoušek, T., Shrestha, R., Kovářová, H., Špánek, R., Sihelská, K., Kokinda, J., Stoulil, J., Steinová, J., Černoušek, T., Shrestha, R., Kovářová, H., Špánek, R., & Alena, Š. (2019). Microbially influenced corrosion of carbon steel in the presence of anaerobic sulphate-reducing bacteria. *Corrosion Engineering, Science and Technology*, *0*(0), 1–11. https://doi.org/10.1080/1478422X.2019.1700642

Chambers, L. D., Stokes, K. R., Walsh, F. C., & Wood, R. J. K. (2006). Modern approaches to marine antifouling coatings. *Surface and Coatings Technology*, *201*, 3642–3652. https://doi.org/10.1016/j.surfcoat.2006.08.129

Chaparro, S. J. S., Darwin, A., Kaksonen, A. H., & Machuca, L. L. (2020). Carbon steel corrosion by bacteria from failed seal rings at an offshore facility. *Scientific Reports*, *10*(12287), 1–15. https://doi.org/10.1038/s41598-020-69292-5

Chen, S., & Zhang, D. (2018). Study of corrosion behavior of copper in 3 . 5 wt .% NaCl solution containing extracellular polymeric substances of an aerotolerant sulphate-reducing bacteria. *Corrosion Science*, *March*, 1–10. https://doi.org/10.1016/j.corsci.2018.03.017

Cheng, Y., Chen, M., Xiao, J., Xing, N., & Huang, C. (2020).

Quantum Chemistry Study on Scale and Corrosion Inhibition Performance of Polyaspartic Acid Quantum Chemistry Study on Scale and Corrosion Inhibition Performance of Polyaspartic Acid. *Earth and Environmental Science*, *571*. https://doi.org/10.1088/1755-1315/571/1/012142

Dagdag, O., Berisha, A., Safi, Z., Dagdag, S., Berrani, M., Jodeh, S., Verma, C., Ebenso, e. eno, Wazzan, N., & El Harfi, A. (2020). Highly durable macromolecular epoxy resin as anticorrosive coating material for carbon steel in 3 % NaCl : Computational supported experimental studies. *Applied Polymer Science*, *e49003*, 1–12. https://doi.org/10.1002/app.49003

Dagdag, O., Berisha, A., Safi, Z., Hamed, O., Jodeh, S., Verma, C., Ebenso, E. E., & El Harfi, A. (2019). DGEBA-polyaminoamide as effective anti-corrosive material for 15CDV6 steel in NaCl medium : Computational and experimental studies. *Journal of Applied Polymer Science*, *48402*, 1–10. https://doi.org/10.1002/app.48402

Dagdag, O., Guo, L., Safi, Z., Verma, C., Ebenso, E. E., Wazzan, N., Masroor, S., Haldhar, R., Jodeh, S., & El Gouri, M. (2020). Epoxy resin and TiO2 composite as anticorrosive material for carbon steel in 3% NaCl medium: Experimental and computational studies. *Journal of Molecular Liquids*, *317*, 114249. https://doi.org/10.1016/J.MOLLIQ.2020.114249

Dagdag, O., Hsissou, R., Berisha, A., Erramli, H., Hamed, O., Jodeh,

S., & El Harfi, A. (2019a). Polymeric-Based Epoxy Cured with a Polyaminoamide as an Anticorrosive Coating for Aluminum 2024-T3 Surface: Experimental Studies Supported by Computational Modeling. *Journal of Bio- and Tribo-Corrosion*, *5*(3), 58. https://doi.org/10.1007/s40735-019-0251-7

Dagdag, O., Hsissou, R., Berisha, A., Erramli, H., Hamed, O., Jodeh, S., & El Harfi, A. (2019b). Polymeric - Based Epoxy Cured with a Polyaminoamide as an Anticorrosive Coating for Aluminum 2024 - T3 Surface : Experimental Studies Supported by Computational Modeling. *Journal of Bio- and Tribo-Corrosion*, *5*(58), 1–13. https://doi.org/10.1007/s40735-019-0251-7

Dagdag, O., Hsissou, R., El harfi, A., El Gana, L., Safi, Z., Guo, L., Verma, C., Ebenso, E. E., & EL Gouri, M. (2020). Development and Anti - corrosion Performance of Polymeric Epoxy Resin and their Zinc Phosphate Composite on 15CDV6 Steel in 3wt % NaCl : Experimental and Computational Studies. *Journal of Bio- and Tribo-Corrosion*, *6*(112). https://doi.org/10.1007/s40735-020-00407-1

Dagdag, O., Safi, Z., Erramli, H., Cherkaoui, O., Wazzan, N., Guo, L., Verma, C., Ebenso, E. E., & El Harfi, A. (2019). Adsorption and anticorrosive behavior of aromatic epoxy monomers on carbon steel corrosion in acidic solution: computational studies and sustained experimental studies. *RSC Advances*, *9*(26), 14782–14796. https://doi.org/10.1039/C9RA01672D

David, E. (2020). The role of iron-oxidizing bacteria in biocorrosion : a review. *The Journal of Bioadhesion and Biofilm Research*, *0*(0), 1–12. https://doi.org/10.1080/08927014.2018.1526281

Dennis, R. V, Patil, V., Andrews, J. L., Aldinger, J. P., & Yadav, G. D. (2015). Hybrid nanostructured coatings for corrosion protection of base metals : a sustainability perspective. *Mater.Res. Express*, *2*(3), 32001. https://doi.org/10.1088/2053-1591/2/3/032001

Dou, W., Liu, J., Cai, W., Wang, D., Jia, R., Chen, S., & Gu, T. (2019). Electrochemical investigation of increased carbon steel corrosion via extracellular electron transfer by a sulfate reducing bacterium under carbon source starvation. *Corrosion Science*, *January*, 1–10. https://doi.org/10.1016/j.corsci.2019.02.005

Etim, I. N., Dong, J., Wei, J., Nan, C., Felix, E., Babu, D., Xu, D., Prasad, A., Su, M., & Ke, W. (2020). Mitigation of sulphate-reducing bacteria attack on the corrosion of 20SiMn steel rebar in sulphoaluminate concrete using organic silicon quaternary ammonium salt. *Construction and Building Materials*, *257*, 119047. https://doi.org/10.1016/j.conbuildmat.2020.119047

Georgiades, E., Scianni, C., Davidson, I., Tamburri, M. N., First, M. R., Ruiz, G., Ellard, K., Deveney, M., & Kluza, D. (2021). The Role of Vessel Biofouling in the Translocation of Marine Pathogens : Management Considerations and Challenges. *Frontiers in Marine Sciences*, *8*(April), 1–20.

https://doi.org/10.3389/fmars.2021.660125

Gu, Y., Yu, L., Mou, J., Wu, D., Xu, M., Zhou, P., & Ren, Y. (2020). Research Strategies to Develop Environmentally Friendly Marine Antifouling Coatings. *Marine Drugs*, *18*, 371. https://doi.org/doi:10.3390/md18070371

Hakim, M. L., Nugroho, B., Nurrohman, M. N., Suastika, I. K., & P, utama I. K. A. (2019). Investigation of fuel consumption on an operating ship due to biofouling growth and quality of anti-fouling coating. *Conference Series: Earth and Environmental Science*. https://doi.org/10.1088/1755-1315/339/1/012037

Hari Kumar, S., & Karthikeyan, S. (2020). A review on self-healing coatings for corrosion protection of metals. *International Journal of Corrosion and Scale Inhibition*, *9*(3), 830–841. https://doi.org/10.17675/2305-6894-2020-9-3-3

Hsissou, R., Abbout, S., Seghiri, R., Rehioui, M., Berisha, A., Erramli, H., Assouag, M., & Elharfi, A. (2020). Evaluation of corrosion inhibition performance of phosphorus polymer for carbon steel in [1 M] HCl : Computational studies (DFT , MC and MD simulations). *J Mater Res Technol*, 1–13. https://doi.org/10.1016/j.jmrt.2020.01.002

Jia, R., Yang, D., Xu, D., & Gu, T. (2017). Anaerobic Corrosion of 304 Stainless Steel Caused by the Pseudomonas aeruginosa Biofilm. *Frontiers in Microbiology*, *8*(November), 1–9.

https://doi.org/10.3389/fmicb.2017.02335

Lejars, M., Margallan, A., & Bressy, C. (2011). Fouling Release Coatings : A Nontoxic Alternative to Biocidal Antifouling Coatings. *Chemical Reviews*. https://doi.org/dx.doi.org/10.1021/cr200350v

Lewandowski, Z., & Beyenal, H. (2008). *Mechanisms of Microbially Influenced Corrosion* (Issue 1, pp. 35–64). https://doi.org/10.1007/7142

Li, Y., & Ning, C. (2019). Bioactive Materials Latest research progress of marine microbiological corrosion and bio- fouling , and new approaches of marine anti-corrosion and anti-fouling. *Bioactive Materials*, *4*(January), 189–195. https://doi.org/10.1016/j.bioactmat.2019.04.003

Little, B. J., Blackwood, D. J., Hinks, J., Lauro, F. . M., Marsili, E., Okamoto, A., Rice, S. A., Wade, S. . A., & Flemming, H. c. (2020). Microbially influenced corrosion — Any progress ? *Corrosion Science*, *170*(25 March), 108641. https://doi.org/10.1016/j.corsci.2020.108641

Liu, H., & Cheng, Y. F. (2018). Mechanistic aspects of microbially in fl uenced corrosion of X52 pipeline steel in a thin layer of soil solution containing sulphate-reducing bacteria under various gassing conditions. *Corrosion Science*, *October 2017*, 0–1. https://doi.org/10.1016/j.corsci.2018.01.029

Martinez, S. (2002). Inhibitory mechanism of mimosa tannin using molecular modeling and substitutional adsorption isotherms. *Materials Chemistry and Physics*, *77*, 97–102.

Mian, S. A., & Khan, Y. (2017). The Adhesion Mechanism of Marine Mussel Foot Protein : Adsorption of L-Dopa on ?- and ? -Cristobalite Silica Using Density Functional Theory. *Journal of Chemistry*, *2017*, 6. https://doi.org/https://doi.org/101155/2017/8756519

Nithya, P., Rameshkumar, S., & sankar, a. (2016). Experimental and Quantum Chemical Studies on the Corrosion Inhibition Performance of A Sysnthesized Schiff Base ... *International Journal of Engineering Science Invention*, *5*(12), 66–74.

Obi-Egbedi, N. O., & Ojo, N. D. (2015). Computational studies of the corrosion inhibition potentials of some derivatives of 1H-Imidazo [4, 5-F] [1, 10] phenanthroline. *Journal of Science Research*, *14*(January), 50–56. https://www.researchgate.net/publication/290324946

Procópio, L. (2019). The role of biofilms in the corrosion of steel in marine environments. *World Journal of Microbiology and Biotechnology*, *4*, 1–8. https://doi.org/10.1007/s11274-019-2647-4

Rajala, P., Huttunen-saarivirta, E., Bomberg, M., & Carpén, L. (2019). Corrosion and biofouling tendency of carbon steel in anoxic groundwater containing sulphate reducing bacteria and

methanogenic archaea. *Corrosion Science*, *July*, 108148. https://doi.org/10.1016/j.corsci.2019.108148

Rathi, P. (2017). Plant Extracts As Green Corrosion Inhibitors in Various Corrosive Media- a Review. *World Journal of Pharmacy and Pharmaceutical Sciences*, 482–514. https://doi.org/10.20959/wjpps20174-8903

Razavi, seyed mohammad, Oh, J., Haasch, richard T., Kim, K., Masoomi, M., Bagheri, R., Slauch, J. M., & Miljkovic, N. (2019). Environment-Friendly Antibiofouling Superhydrophobic Coatings [Research-article]. *ACS Sustainable Chemistry & Engineering*, *7*, 14509–14520. https://doi.org/10.1021/acssuschemeng.9b02025

Sachan, R., Kumar, A., Yuvraj, S., & Negi, S. (2020). Study of Microbially Influenced Corrosion in the Presence of Iron - Oxidizing Bacteria (Strain DASEWM2). *Journal of Bio- and Tribo-Corrosion*, 1–14. https://doi.org/10.1007/s40735-020-00409-z

Sachan, R., & Singh, A. K. (2018). Corrosion of steel due to iron oxidizing bacteria. *Anti-Corrosion Methods and Materials*. https://doi.org/10.1108/ACMM-05-2018-1928

Soliman, T., & Inglis, G. J. (2018). Forecasting the economic impacts of two biofouling invaders on aquaculture production of green-lipped mussels Perna canaliculus in New Zealand. *Aquacult Environ Interac*, *10*, 1–12.

https://doi.org/https://doi.org/10.3354/aei00249

Suleiman, R., & El, B. (2015). RSC Advances Novel hybrid epoxy silicone materials as e ffi cient anticorrosive coatings for mild steel. *RSC Advances*, *5*, 39155–39167. https://doi.org/10.1039/C5RA04500B

Umoren, S. A., Solomon, M. M., & Saji, V. S. (2020). *Corrosion Inhibitors for Sour Oilfield Environment (H 2 S Corrosion)*.

Urbahs, A., Savkovs, K., Rijkuris, G., & Andrejeva, D. (2018). Corrosion and Wear Analysis in Marine Transport Constructions. *Transport and Aerospace Engineering*, *6*(1), 5–14. https://doi.org/10.1515/tae-2018-0001

Uwakwe, K. J., Okafor, P. C., Obike, A. I., & Ikeuba, A. I. (2016). Molecular dynamics simulations and quantum chemical calculations for the adsorption of some imidazoline derivatives on iron surface. *Global Journal of Pure and Applied Sciences*, *23*, 69–80. https://doi.org/https://dx.doi.org/10.4314/gipas.v23i1.8

Vinagre, P. A., Simas, T., Cruz, E., Pinori, E., & Svenson, J. (2020). Marine Biofouling : A European Database for the Marine Renewable Energy Sector. *Journal of Marine Science and Engineering*.

Wang, D., Unsal, T., Kumseranee, S., Punpruk, S., Mohamed, M. E., Saleh, M. A., & Gu, T. (2021). Sulfate reducing bacterium Desulfovibrio vulgaris caused severe microbiologically influenced

corrosion of zinc and galvanized steel. *International Biodeterioration & Biodegradation*, *157*(September 2020), 105160. https://doi.org/10.1016/j.ibiod.2020.105160

Wang, L., Tang, C., Wang, X., & Zheng, W. (2019). Molecular dynamics simulation on the thermodynamic properties of insulating paper cellulose modified by silane coupling agent grafted nano-SiO2. *AIP Advances*, *9*, 125134. https://doi.org/10.1063/1.5131821

Weinhold, M., Soubatch, S., Temirov, R., Rohlfing, M., Jastorff, B., & Tautz, F. S. (2006). Structure and Bonding of the Multifunctional Amino Acid L -DOPA on Au (110). *J. Phys. Chem. B*, *110*(47), 23756–23769. https://doi.org/10.1021/jp064956t CCC:$33.50

Xie, C., Li, C., Xie, Y., Cao, Z., Li, S., Zhao, J., & Wang, M. (2020). ZnO / Acrylic Polyurethane Nanocomposite Superhydrophobic Coating on Aluminum Substrate Obtained via Spraying and Co-Curing for the Control of Marine Biofouling Biofouling is a costly and complex problem in the marine industry . Traditional anti-. *Surfaces and Interfaces*, 100833. https://doi.org/10.1016/j.surfin.2020.100833

Xie, C., Li, C., Xie, Y., Cao, Z., Li, S., Zhao, J., & Wang, M. (2021). ZnO/Acrylic Polyurethane Nanocomposite Superhydrophobic Coating on Aluminum Substrate Obtained via Spraying and Co-Curing for the Control of Marine Biofouling. *Surfaces and*

Interfaces, *22*, 100833. https://doi.org/10.1016/j.surfin.2020.100833

Zhang, T., Wang, J., Li, G., & Liu, H. (2021). Crevice corrosion of X80 carbon steel induced by sulfate reducing bacteria in simulated seawater. *Bioelectrochemistry*, 107933. https://doi.org/10.1016/j.bioelechem.2021.107933

Zhao, Y., Zhou, E., Xu, D., Yang, Y., Zhao, Y., Zhang, T., Gu, T., Yang, K., & Wang, F. (2018). SC. *Corrosion Science*. https://doi.org/10.1016/j.corsci.2018.08.018